HGG Advances

REPORT

Variants in *LSM7* impair LSM complexes assembly, neurodevelopment in zebrafish and may be associated with an ultra-rare neurological disease

Alexa Derksen,[1,2,3,16] Hung-Yu Shih,[4,16] Diane Forget,[2] Lama Darbelli,[1] Luan T. Tran,[1] Christian Poitras,[2] Kether Guerrero,[1] Sundaresan Tharun,[5] Fowzan S. Alkuraya,[6] Wesam I. Kurdi,[7] Cam-Tu Emilie Nguyen,[8] Anne-Marie Laberge,[9] Yue Si,[10] Marie-Soleil Gauthier,[2] Joshua L. Bonkowsky,[4,11,17] Benoit Coulombe,[2,13,17] and Geneviève Bernard[1,3,12,14,15,17,*]

Summary

Leukodystrophies, genetic neurodevelopmental and/or neurodegenerative disorders of cerebral white matter, result from impaired myelin homeostasis and metabolism. Numerous genes have been implicated in these heterogeneous disorders; however, many individuals remain without a molecular diagnosis. Using whole-exome sequencing, biallelic variants in *LSM7* were uncovered in two unrelated individuals, one with a leukodystrophy and the other who died *in utero*. LSM7 is part of the two principle LSM protein complexes in eukaryotes, namely LSM1-7 and LSM2-8. Here, we investigate the molecular and functional outcomes of these *LSM7* biallelic variants *in vitro* and *in vivo*. Affinity purification-mass spectrometry of the LSM7 variants showed defects in the assembly of both LSM complexes. *Lsm7* knockdown in zebrafish led to central nervous system defects, including impaired oligodendrocyte development and motor behavior. Our findings demonstrate that variants in *LSM7* cause misassembly of the LSM complexes, impair neurodevelopment of the zebrafish, and may be implicated in human disease. The identification of more affected individuals is needed before the molecular mechanisms of mRNA decay and splicing regulation are added to the categories of biological dysfunctions implicated in leukodystrophies, neurodevelopmental and/or neurodegenerative diseases.

Leukodystrophies encompass a group of rare genetic neurodevelopmental and neurodegenerative disorders affecting cerebral white matter. Recent advances in genetics and neuroimaging have led to the discovery of many subtypes that are clinically and genetically heterogeneous.[1–3] These diseases can be classified based on specific brain magnetic resonance imaging (MRI) patterns as either hypomyelinating or non-hypomyelinating. Hypomyelinating leukodystrophies are associated with abnormal myelin formation during development, whereas non-hypomyelinating leukodystrophies are associated with abnormal myelin homeostasis.[4,5] These heterogenous diseases collectively affect as many as 1 in 7,600 individuals, with a broad range of onset spanning from prenatal life to late adulthood.[6–8] Although the era of next-generation sequencing (NGS) has facilitated rare disease diagnosis, 20%–30% of individuals with leukodystrophies remain genetically undiagnosed.[2,9,10] These individuals and their families often undergo extensive diagnostic odysseys, which adversely impacts their wellbeing and healthcare.[11,12]

Leukodystrophies were initially identified and classified predominantly as disorders of myelin production or turnover, for example Pelizaeus-Merzbacher disease (MIM: 312080) and metachromatic leukodystrophy (MIM: 250100).[8] Recent advances in research have revealed that pathogenic variants in many transcription- and translation-related genes are implicated in white matter pathologies. For example, it is well-established that pathogenic variants in the genes encoding RNA polymerase III subunits (i.e., *POLR3A* [MIM: 614258], *POLR3B* [MIM: 614366], *POLR1C* [MIM: 610060], and *POLR3K* [MIM: 606007]) as well as tRNA synthetase genes (i.e., *EPRS1* [MIM: 138295], *RARS1* [MIM: 107820], *VARS1* [MIM: 192150], etc.) are associated with white matter disorders.[13–19]

LSM proteins ("like Sm") are a family of proteins that form multi-subunit complexes that interact directly with RNA.[20–24] The 8 main LSM proteins (LSM1-8) form two heteroheptameric ring-shaped complexes composed of different subunits. More specifically, the LSM1 through

[1]Child Health and Human Development Program, Research Institute of the McGill University Health Centre, Montréal, QC H4A 3J1, Canada; [2]Translational Proteomics Laboratory, Institut de Recherches Cliniques de Montréal, Montréal, QC H2W 1R7, Canada; [3]Department of Neurology and Neurosurgery, McGill University, Montréal, QC H3A 0G4, Canada; [4]Department of Pediatrics, University of Utah School of Medicine, Salt Lake City, UT 84132, USA; [5]Department of Biochemistry, Uniformed Services University of Health Sciences (USUHS), Bethesda, MD 20814, USA; [6]Department of Genetics, King Faisal Specialist Hospital and Research Centre, Riyadh 12713, Saudi Arabia; [7]Department of Obstetrics and Gynecology, Maternal Fetal Medicine, King Faisal Specialist Hospital and Research Centre, Riyadh 12713, Saudi Arabia; [8]Neurosciences Department, Université de Montréal, Montréal, QC H3T 1J4, Canada; [9]Service de Génétique Médical, CHU Sainte-Justine, Montréal, QC H3T 1C5, Canada; [10]GeneDx, Gaithersburg, MD 20877, USA; [11]Brain and Spine Center and Primary Children's Center for Personalized Medicine, Primary Children's Hospital, Salt Lake City, UT 84113, USA; [12]Department of Pediatrics, McGill University, Montréal, QC H3A 0G4, Canada; [13]Department of Biochemistry and Molecular Medicine, Université de Montréal, Montréal, QC H3T 1J4, Canada; [14]Department of Human Genetics, McGill University, Montréal, H3A 0G4, Canada; [15]Division of Medical Genetics, Department of Specialized Medicine, McGill University Health Centre, Montréal, QC H4A 3J1, Canada
[16]These authors contributed equally
[17]These authors contributed equally
*Correspondence: genevieve.bernard@mcgill.ca
https://doi.org/10.1016/j.xhgg.2021.100034.

LSM7 proteins form the LSM1-7 complex, and the LSM2 through LSM8 proteins form the LSM2-8 complex. The LSM1-7 complex interacts with the mRNA processing and degradation factor protein PATL1, localizing to the cytoplasmic processing bodies (P-bodies), and plays a role in mRNA decay.[20,21,24] Eukaryotic cytosolic mRNA decay, a well-characterized and highly conserved process, occurs via one of two pathways, both beginning with the shortening of the poly(A) tail and followed by degradation in either the 3′–5′ or 5′–3′ direction.[21,23,24] Studies in yeast revealed that the LSM1-7 complex likely acts as an enhancer of decapping in the 5′–3′ pathway, as cells with variants in Lsm1p through Lsm7p block mRNA decay at the decapping step.[21,25,26] Conversely, the LSM2-8 complex is localized to the nucleus, where it interacts with U6 small nuclear RNA (snRNA), which is the catalytic component of the primary spliceosome.[20,22,23] Splicing is a multi-step reaction involving the interaction and subsequent rearrangements of the 5 primary spliceosomal snRNAs (U1, U2, U4, U5, and U6) and their protein interactors.[25–29] The LSM2-8 complex acts as a chaperone for U6 snRNA, supporting its rearrangements during splicing and its recycling following the spliceosome reaction.[30,31] Thus, the LSM1-7 and LSM2-8 complexes play critical roles in the highly regulated cellular mechanisms of mRNA decay and splicing, respectively.[20]

Here, we report two individuals with biallelic variants in *LSM7* (MIM: 607287), one with a clinical diagnosis of leukodystrophy and the other who died *in utero*. These *LSM7* variants were investigated on a molecular and functional level to evaluate their impact on the LSM complexes. A zebrafish model was also created to study the functional impact of wild-type (WT) and mutant LSM7 on the development of the central nervous system (CNS).

This project was approved by the Research Institute of the McGill University Health Centre Research Ethics Board (PED-11-105, 2019-4972), and informed consent was obtained from all participants in this study. The first affected individual was referred at the age of 3 years for neurological assessment at the McGill University Health Center. He presented with spastic quadriparesis, white matter anomalies, developmental delay, progressive sensorineural hearing loss, hypospadias, and feeding difficulties. He is currently 7 years old and wheelchair bound. His MRIs showed cerebellar hypoplasia and progressive white matter signal abnormalities between 17 and 35 months, indicative of a leukodystrophy (Figure 1). To determine the genetic cause, massive parallel (NextGen) sequencing on an Illumina system was performed by GeneDx as previously described,[32] using DNA isolated from saliva samples of the affected individual and his parents. The quality threshold of the exome sequencing for this individual was 98.4%, with a mean depth of coverage of 88 reads. Analysis was completed using the general assertion criteria for variant classification and is publicly available on the GeneDx ClinVar submission page. A second analysis of the sequence variants was conducted in-house at the Research Institute of the McGill University Health Centre. Sequence variants were prioritized using the standards and guidelines for interpretation set out by the American College of Medical Genetics (ACMG).[33] These analyses revealed a homozygous variant in *LSM7* (GenBank: NM_016199.2; GRCh37/hg19) at position c.121G>A (p.Asp41Asn) (chr19: 2324172C>T) as a strong candidate for pathogenicity (Figures 2A and 2B). Targeted Sanger sequencing confirmed the presence of the variant as homozygous in the affected individual, with both parents being carriers (Figure 2D). Subsequently, a second individual was found through GeneMatcher.[34,35] This family was referred for genetic investigations following recurrent fetal deaths. The proband died *in utero* at 32 weeks of gestation and was found to have thick nuchal translucency and encephalocele. Karyotyping was performed in 3 of the pregnancies that ended in fetal death and revealed no chromosomal abnormalities. Duo exome sequencing of the consanguineous parents was conducted as previously described[36] and revealed that both parents were carriers of the same variant in *LSM7* at position c.206G>C (p.Arg69Pro) (chr19: 2321785C>G). The parents were not found to both be carriers for any known recessive diseases, and no other gene candidate was identified. Their chromosomal analyses were also normal. The multiple fetal deaths are thereby presumed to be caused by the homozygous variant in *LSM7*. Unfortunately, DNA was not available from the fetuses or the 3 healthy children of this couple for sequencing.

Both *LSM7* variants are present in highly conserved amino acid residues (Figure 2C) and are classified as rare. The p.Asp41Asn variant was observed only 9 times as heterozygous in 232,800 alleles in large population cohorts[37] (minor allele frequency 3.87e−5), while the p.Arg69Pro variant has never been reported in large population control databases. *In silico* genetic analysis predict both variants to be deleterious on protein structure and function (p.Asp41Asn: Mutation Taster 0.99, CADD 28.8, Provean −4.61, SIFT 0.001; p.Arg69Pro: Mutation Taster 0.99, CADD 24.9, Provean −7.00, SIFT 0.00) (Table S1).[38–42]

To examine these variants at a molecular level, we performed RT-qPCR and immunoblot using RNA and protein extracts (n = 6) from fibroblasts of the first affected individual as well as two age- and sex-matched healthy control individuals. RT-qPCR primers were designed and efficiency tested in accordance with the Minimum Information for Publication of Quantitative Real-Time PCR Experiments (MIQE) guidelines.[43,44] All data were normalized to *SDHA* (MIM: 600857) or *RPL30* (MIM: 180467) using the ΔΔCt method, which revealed reduced levels of *LSM7* mRNA ($p < 0.01$) in affected individual 1 compared to control individuals (Figure 3A). Immunoblots were performed on protein extracts using antibodies targeting LSM7 (Abcam 241656, dilution 1:10,000) and beta-tubulin (Abcam 6046, dilution 1:20,000), followed by incubation with a polyclonal goat anti-rabbit IgG (H+L) (Novus Biologicals, dilution 1:5,000) antibody and visualization using

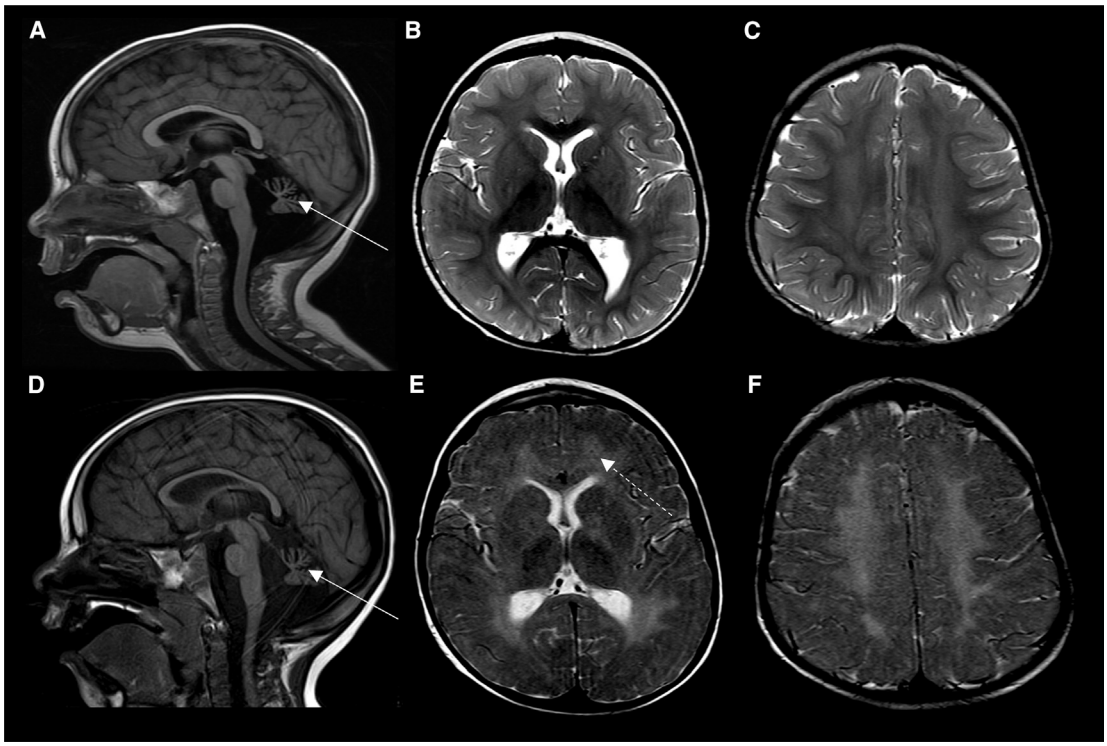

Figure 1. MRI characteristics of individual 1
Brain MRI of individual 1 at 17 months (A–C) and 35 months of age (D–F).
(A) and (D) Sagittal T1-weighted images at the midline showing cerebellar hypoplasia (thin arrows).
(B, C, E, and F) Axial T2-weighted images at the level of the basal ganglia (B and E) and *centrum semiovale* (C and F) showing progressive diffuse demyelination (dotted arrow).

Amersham ECL Western Blot Detecting Reagent according to manufacturer's protocol (GE Life Sciences). Band intensity was quantified using ImageJ software, and statistical significance was determined using a parametric, unpaired t test (two tailed). A decreased amount of LSM7 protein ($p < 0.001$) was seen in the affected individual as compared to control individuals (Figures 3B and 3C). Samples from the fetuses described in the second family (p.Arg69Pro) were not available for analysis.

In order to evaluate the impact of these variants on the formation of the LSM complexes, we generated structural models of wild-type and mutant yeast Lsm1-7 (PDB: 4M75)[45] and Lsm2-8 complexes (PDB: 4M77)[45] using PyMOL Molecular Graphics System, version 2.0 Schrödinger (Figures 2E and 2F). All the LSM proteins (LSM1 through LSM8) are highly conserved from yeast to humans. Based on their homology, we mapped the human variants at positions Asp41 and Arg69 to their corresponding yeast residues at Asp56 and Arg87, respectively. Using PyMOL, we modeled the effects of the predicted deleterious variants. The first variant, p.Asp56Asn in yeast, is predicted to result in the loss of polar contacts with other Lsm7 residues in both the Lsm1-7 and Lsm2-8 complexes (Figures S1A–S1D). Meanwhile, the second variant, p.Arg87Pro in yeast, is predicted to result in the loss of polar contacts with Lsm7 residues and a residue on the neighboring Lsm5 protein in both the Lsm1-7 and Lsm2-8 complexes (Figures S1E–S1H). Based on this modeling, we predicted that each of these substitutions would lead to a compromised ability of Lsm7 to interact with the other Lsm subunits, and consequently, the assembly of the Lsm1-7 and Lsm2-8 complexes would be significantly impaired.

To determine the potential pathogenic role of these variants, we assessed their impact on the assembly of the LSM1-7 and LSM2-8 complexes in human cells. A FLAG-tagged version of the wild-type LSM7, as well as that containing either the p.Asp41Asn or p.Arg69Pro variant, were produced transiently in HEK293 cells. Anti-FLAG affinity purification was conducted on cell extracts according to standard procedures in 4 independent replicate experiments.[46,47] The protein extracts were digested with trypsin, and the resulting tryptic peptides were purified and identified using liquid chromatography-tandem mass spectrometry (LC-MS/MS) with a high-performance liquid chromatography (HPLC) system coupled to Orbitrap fusion mass spectrometer (Thermo Scientific) through a Nanospray Flex Ion Source. Protein database searching was performed using MaxQuant version 1.6.10.43[48–53] against the SwissProt human protein database downloaded on April 4, 2019. Known affinity purification mass spectrometry (AP-MS) protein contaminants including keratins were excluded, and protein intensities were analyzed using Perseus version 1.6.10.43.[54–57] Proteins not present in at least 3 out of 4 replicates were excluded. Wild-type,

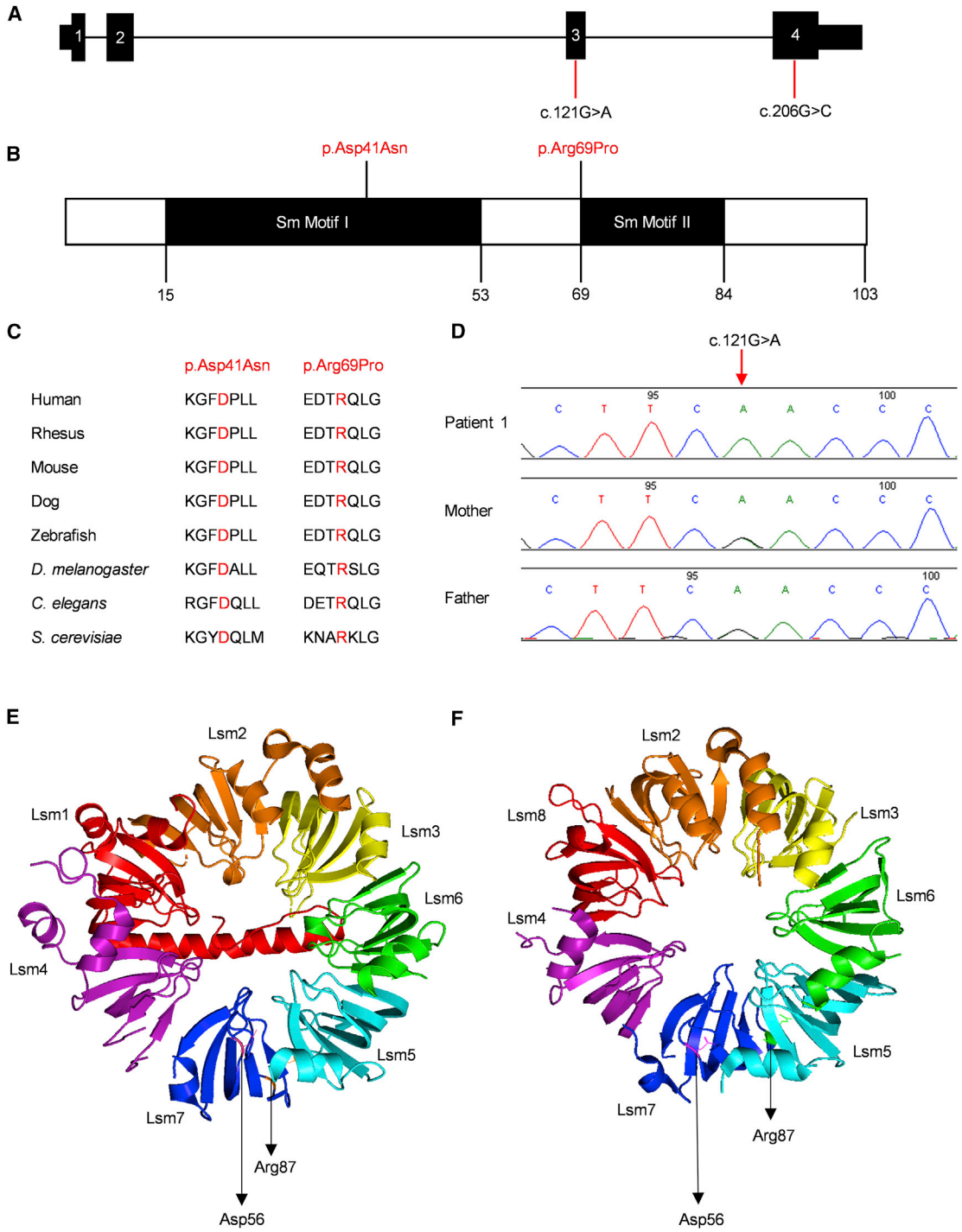

Figure 2. Biallelic variants in *LSM7*

(A) Genomic organization of *LSM7* in humans (UCSC Genome Browser hg19) with the position of the pathogenic variants within the *LSM7* gDNA indicated.

(B) Major motifs of the 103 amino acid LSM7 protein with position of variants indicated.

(C) LSM7 variants in affected individuals are at conserved amino acid residues.

(D) *LSM7* gene sequencing of affected individual 1 and parents.

(E and F) 3D representations (created with PyMOL) of yeast (E) Lsm1-7 and (F) Lsm2-8 complexes displaying location of variants.

p.Asp41Asn, and p.Arg69Pro proteins were compared against FLAG empty vector control samples and were labeled as high-confidence interactors when their adjusted p values were under 0.05 and their intensity ratios over 2. The p values were adjusted for multiple hypothesis testing with a permutation-based approach using an s0 correction factor of 0.1 with 10,000 iterations.[58] A Student's t test was performed between p.Asp41Asn and p.Arg69Pro against

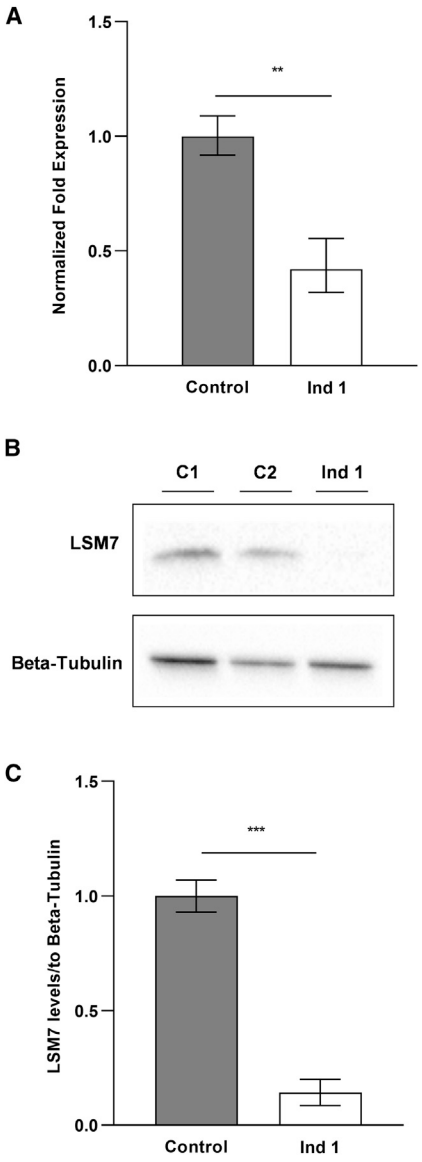

Figure 3. LSM7 mRNA and protein levels are decreased in individual 1 compared to control individuals

(A) RT-qPCR analysis of *LSM7* mRNA extracted from individual 1's fibroblasts and two age- and sex-matched control individuals (n = 6). The results are represented in terms of fold change after normalizing to *RPL30* and *SDHA* mRNAs. Each value represents the mean ± SEM (unpaired t test [two tailed] **$p < 0.01$).

(B) Total protein lysates extracted from individual 1 and age- and sex-matched control individual fibroblasts were immunoblotted with anti-LSM7 and anti-beta-tubulin.

(C) The pixel densities of immunoblot bands from at least 3 independent replicates were quantified using ImageJ software, normalized over beta-tubulin immunoblot and represented as mean ± SEM (unpaired t test [two tailed], ***$p < 0.001$).

the wild-type samples. These results revealed that cells producing the wild-type LSM7 protein resulted in the co-precipitation of all the LSM1-7 and LSM2-8 complex subunits, along with multiple other known interactors of these complexes (Figures 4A and 4B). However, pull-downs from lysates of HEK293 cells producing the p.Asp41Asn or p.Arg69Pro variants revealed dramatically reduced association of the mutated LSM7 protein with the other LSM proteins constituting the LSM1-7 and LSM2-8 complexes. Consistent with this defect, most of the known interactors of these complexes were also not pulled down in the mutant strains (Figure 4C). The LSM1-7 and LSM2-8 complexes are known to interact with many mRNA decay and splicing factors, respectively. Relative to the FLAG-tagged wild-type LSM7, the p.Asp41Asn and p.Arg69Pro mutants showed reduced interaction with the mRNA decay factors PATL1 and EDC4 as well as with triple small nuclear ribonucleoprotein (tri-snRNP) factors including PRPF3, PRPF4, SART3, and SNRNP200. These splicing factors are required for the formation of the U4/U6/U5 tri-snRNP complex, an important precursor in the major spliceosome reaction.[59–61] Similarly, PATL1 is a highly conserved interacting partner of the LSM1-7 complex that plays a key role in mRNA decay.[62] Thus, these findings suggest that both variants lead to defects in the assembly of the LSM1-7 and LSM2-8 complexes and result in the subsequent loss of key complex interactors.

Since the levels of LSM7 protein were found to be decreased in affected individual 1 compared to control individuals (Figure 3C), we predicted that the defect in LSM1-7 and LSM2-8 complex assembly could be further exacerbated by reduced starting levels of the mutant LSM7 protein. In our LC-MS/MS experiments, when the levels of FLAG-tagged mutant LSM7 were normalized to that of the FLAG-tagged wild-type, we found that both mutated subunits pulled down relatively lower amounts of the other LSM complex subunits. Therefore, reduced protein levels of mutant LSM7, as seen in affected individual 1, could potentially intensify the defects we observed in our LC-MS/MS experiments. We also saw reduced levels of *LSM7* mRNA in this individual compared to control individuals (Figure 3A). Since the levels of the LSM2-8 complex are expected to be lower in this individual (Figure 4C), reduced *LSM7* transcript levels could result from inefficient splicing of *LSM7* pre-mRNA. Several other studies have shown that both missense and synonymous variants can impact RNA structure, stability, folding, microRNA (miRNA) binding, splicing regulatory sites, and/or translation efficiency.[63–65] Therefore, we hypothesize that this missense variant could alter the *LSM7* pre-mRNA, further targeting it for degradation and thereby reducing transcript levels.

To demonstrate the functional impact of wild-type and mutant *LSM7*, a zebrafish model was created and used to study the impact of LSM7 hypofunction on CNS development. The zebrafish experiments were performed in strict accordance with relevant institutional and national guidelines and regulations. Adult fish were bred according to standard methods, and embryos were raised at 28.5°C in E3 embryo medium and staged by time and morphology. The zebrafish ortholog *lsm7* (ENSDART00000081188.7) and human *LSM7* share significant homology. The zebrafish Lsm7 protein has 95% amino acid identity with human LSM7, including conservation of the two amino

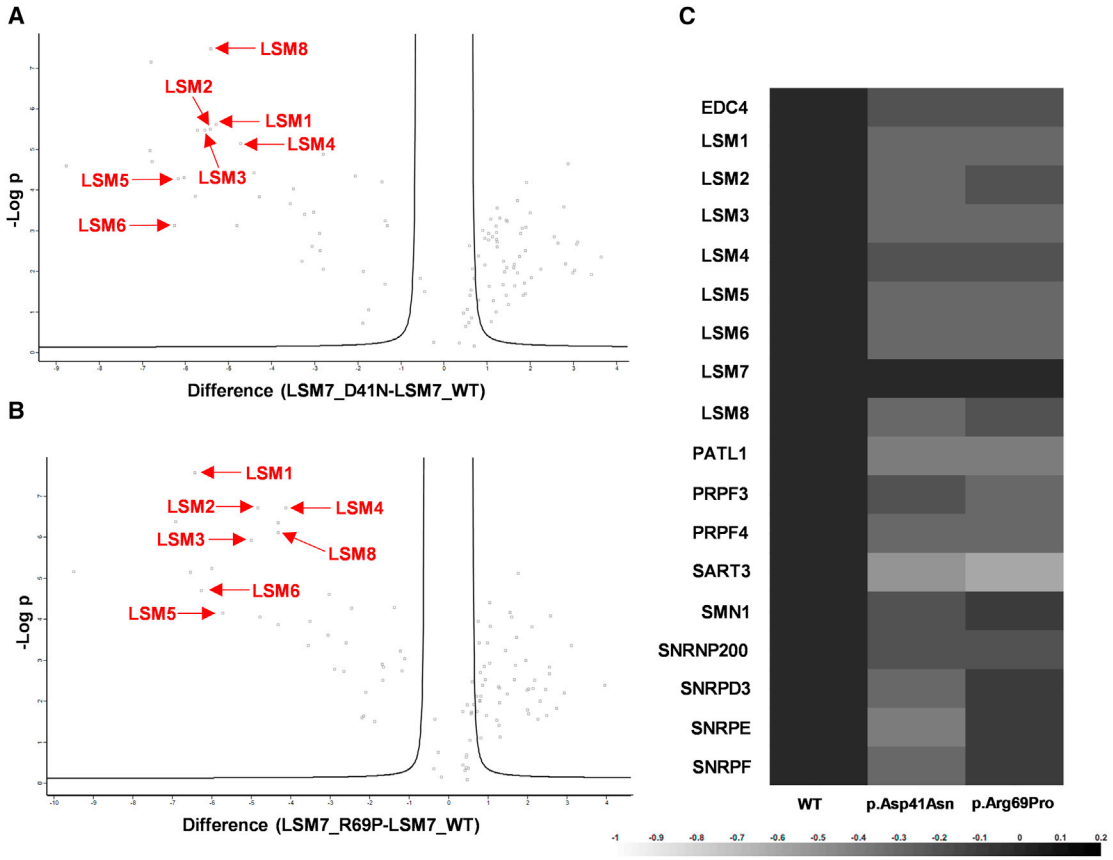

Figure 4. Impact of LSM7 variants on LSM1-7 and LSM2-8 complex assembly
(A and B) Volcano plots of the $\log_2$-transformed MaxQuant ratios of the p.Asp41Asn or p.Arg69Pro/wild-type (x axis) and the $-\log_{10}$-transformed p values (adjusted with permutation-based false discovery rate) resulting from the two-tailed two-sample Student's t tests. (C) Heatmap contains the MaxQuant ratios for the subunits of the LSM complexes and known important complex interactors.

acid residues of the variants in the affected individuals (p.Asp41Asn and p.Arg69Pro) (Figure 5A). We evaluated *lsm7* gene expression using an antisense digoxigenin-uridine triphosphate (UTP) labeled riboprobe, which was synthesized according to the manufacturer's instructions (Roche). *In situ* hybridizations were performed as previously described[66] from 1 day post-fertilization (dpf) to 5 days post-fertilization, and the color reaction was carried out using NBT/BCIP substrate (Roche). At 1 day post-fertilization and 2 days post-fertilization, the *lsm7* transcript was detected in the developing brain, spinal cord, and eye (Figure 5B). By 3 days post-fertilization and persisting through 5 days post-fertilization, expression was present in the olfactory bulb, cerebellum, and hindbrain (Figure 5B).

To investigate the physiological function of Lsm7 in an animal model of neurodevelopment, we used CRISPR-Cas9 gene editing to develop Lsm7-Crispant zebrafish lacking functional Lsm7 protein. Single guide RNA (sgRNA) target sites for the zebrafish *lsm7* gene (Ensembl Zv11: ENSDART00000081188.7) were designed and off-target effects checked. Co-injection of *lsm7* exon 3 sgRNA (460 pg) and Cas9 protein (460 pg, PNA BIO) was done on one-cell-stage embryos and efficiently induced insertions and deletions as determined by high-resolution melting analysis (HRMA) PCR (Figure S2).

Embryos injected with *lsm7* sgRNA and Cas9 protein showed impaired nervous system development and normal lifespan (1.6% lethality, n = 128). We categorized the surviving embryos into two phenotypes according to the severity: a mild phenotype who displayed normal trunk morphology but brain and eye size reduction, and a moderate phenotype exhibiting a bent trunk, edema in the pericardial sac, and decreased eye and brain size (Figures 5C–5E). At 5 days post-fertilization the fish larvae were fixed, and one eye was dissected out, mounted laterally, and imaged. The eye size was measured along the horizontal axis using ImageJ software (Figure 5E, dashed line) in Lsm7-Crispants (injected with *lsm7* sgRNA and Cas9 protein). Eye diameter was found to be significantly reduced in Lsm7-Crispants compared to controls ($p < 0.001$) (Figures 5E and 5F). We also evaluated motor behavior of Lsm7-Crispants by analyzing the response to light stimuli at 7 days post-fertilization in 96-well square bottom plates (Krackeler Scientific) using video analysis software (Noldus EthoVision). We found that larvae response to light stimuli was significantly reduced in the Lsm7-Crispants ($p < 0.001$) (Figure 5G).

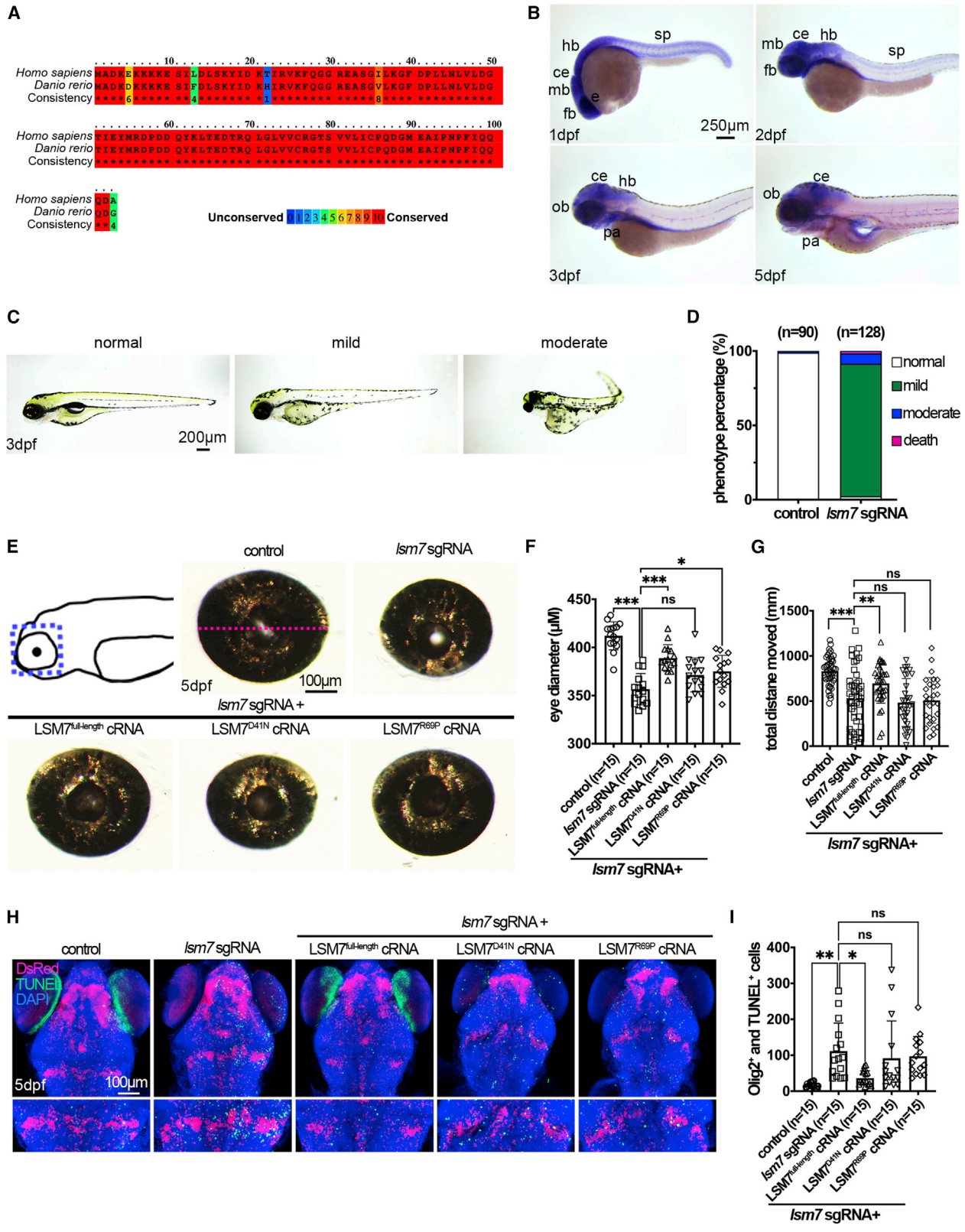

Figure 5. The zebrafish *Lsm7* ortholog is highly conserved with human *LSM7*, is expressed in developing nervous system, and is necessary for embryonic morphology, eye size, motor behavior, and survival of oligodendrocytes

(A) Amino acid alignment of human and zebrafish *LSM7* sequences. Identical residues are marked by red boxes, and percent similarity is shown by different colors.

(B) *In situ* hybridization was performed for detecting *lsm7* expression during zebrafish embryogenesis. Embryo stages are shown in the bottom left of each panel. All panels display the lateral view, with dorsal to the top and rostral to the left.

(C) Phenotypes of *lsm7*-Crispants.

(legend continued on next page)

To explore the effects of the mutant LSM7 proteins, capped RNA (cRNA) encoding the full coding sequence of $LSM7^{full\text{-}length}$, $LSM7^{Asp41Asn}$, or $LSM7^{Arg69Pro}$ were prepared. The eye phenotype could be rescued by concomitant injection of human $LSM7^{full\text{-}length}$ and $LSM7^{Arg69Pro}$ cRNAs, but not by the $LSM7^{Asp41Asn}$ cRNA (Figures 5E and 5F). Since the p.Asp41Asn variant is located on a conserved RNA contacting residue in the Sm motif-I of LSM7, the inability of the $LSM7^{Asp41Asn}$ cRNA to rescue the eye size phenotype of the Lsm7-Crispants implies that RNA processing activity is critical for eye development. Furthermore, the movement deficits observed in the Lsm7-Crispants could only be rescued with the $LSM7^{full\text{-}length}$ cRNA but not by either of the mutant cRNAs ($LSM7^{Arg69Pro}$ or $LSM7^{Asp41Asn}$), indicating that both mutants impact motor behavior (Figure 5G). Overall, these findings demonstrate that *lsm7* knockdown zebrafish have phenotypic characteristics similar to those observed in the first affected individual.

On a cellular level using our zebrafish model, we explored the role of *LSM7* on the development and survival of oligodendrocytes, the myelin-producing cells of the CNS, which are primarily implicated in leukodystrophies. We used the transgenic line Tg (*olig2:dsRed*) to label oligodendrocytes, oligodendrocyte precursor cells (OPCs), and motor neurons and compared cell counts in larvae injected with wild-type $LSM7^{full\text{-}length}$ cRNA to $LSM7^{Asp41Asn}$ or $LSM7^{Arg69Pro}$ cRNAs. The immunohistochemistry was performed as previously described[67] using rabbit anti-dsRed (Clontech, dilution 1:250), Alexa 555 goat anti-rabbit (ThermoFisher Scientific, dilution 1:400), and 4′,6-diamidino-2-phenylindole (DAPI). Additionally, terminal deoxynucleotidyl transferase deoxyuridine triphosphate (dUTP) nick-end labeling (TUNEL) was performed on whole-mount larvae (ApopTag Fluorescein *In Situ* Apoptosis Detection Kit; Millipore) as previously described.[68] Confocal imaging was used and cells counted using Photoshop's (Adobe) count tool. We found that apoptosis of oligodendrocytes was significantly increased in Lsm7-Crispants ($p < 0.01$) (Figures 5H and 5I) and could be rescued by concomitant injection of $LSM7^{full\text{-}length}$ cRNA but not by the $LSM7^{Asp41Asn}$ or $LSM7^{Arg69Pro}$ cRNAs (Figures 5H and 5I). This suggests a role for *LSM7* in oligodendrocyte survival and demonstrates that both variants are associated with an increase in apoptosis of oligodendrocytes. Interestingly, the hypoplastic cerebellum in individual 1 corresponded to the small cerebellar phenotype observed in Lsm7-Crispants. It is possible that deficiency or dysregulation of LSM7 in the cerebellum of the first affected individual at key developmental stages could contribute to the observed cerebellar hypoplasia. Overall, this zebrafish model has allowed us to identify a relationship between LSM7 and CNS development, as well as oligodendrocyte survival, thus providing further evidence of a link to leukodystrophies, genetic neurodevelopmental and/or neurodegenerative disorders.

Our current data do not allow us to understand why one variant (p.Arg69Pro) led to *in utero* death, while the other variant (p.Asp41Asn) leads to a less severe phenotype. Samples were unavailable from the fetuses described in the second family for mRNA or protein analysis, limiting direct functional studies. However, the p.Arg69Pro variant, but not p.Asp41Asn, is predicted to be located at an exon-intron boundary by MutationTaster,[42] which could impair or cause dysfunction in pre-mRNA splicing. For this reason, we hypothesize that perhaps the p.Arg69Pro variant causes splice site changes that are detrimental and cause embryonic lethality. Specific splicing variants can cause cell-specific defects, as in the case of individuals presenting with a unique phenotype of basal ganglia abnormalities and the same pathogenic splicing variant in *POLR3A*.[69–73] This further supports a possible association between distinct splicing defects and phenotypic heterogeneity within individuals with pathogenic variants in the same gene. While a splicing defect could offer support for the difference in phenotypic severity, we would be unable to confidently conclude that it is indeed the only factor at play. There have been several reports in the literature of individuals with the same variant presenting with large discordances in phenotypic severity. One such report describes a sibling pair with the same compound heterozygous variants in *POLR1C*, which led to neonatal death in one sibling, while the other remains alive and is much less affected.[74] Another example is presented in an inbred family where the same variant in *SLC17A5* results in either a mild or severe phenotype.[75]

In summary, this study identified *LSM7*, a gene involved in the processes of 5′–3′ mRNA decay and splicing,[20] as playing a role in the development of the CNS and in oligodendrocyte survival. Before a definite association between *LSM7* variants and leukodystrophy, genetic neurodevelopmental and/or neurodegenerative disease can be made, more affected individuals with biallelic variants in *LSM7* need to be identified. Our findings, however, add this

(D) Quantification of control and *lsm7*-Crispants by phenotype severity.
(E) Top left panel shows a cartoon representation of the dissected region of larvae (blue dashed line rectangle). Images of eyes of control, *lsm7*-Crispant, $LSM7^{full\text{-}length}$ cRNA-, $LSM7^{R69P}$ cRNA-, and $LSM7^{D41N}$ cRNA-rescued larvae are shown. The eye diameter was measured as indicated by the magenta dashed line shown on control eye.
(F) Quantification of eye size.
(G) Motor swimming behavior of the control, *lsm7*-Crispant, $LSM7^{full\text{-}length}$ cRNA-, $LSM7^{R69P}$ cRNA-, and $LSM7^{D41N}$ cRNA-rescued larvae at 7 dpf.
(H) Confocal images of dorsal view of the control, *lsm7*-Crispant, $LSM7^{full\text{-}length}$ cRNA-, $LSM7^{R69P}$ cRNA-, and $LSM7^{D41N}$ cRNA-rescued larvae with rostral to the top. Lower panels are enlarged region from upper panels for apoptotic cell quantification.
(I) Quantification of the number of TUNEL and DsRed double-positive cells of (H). Abbreviations: ce, cerebellum; dpf, days post-fertilization; fb, forebrain; hb, hindbrain; mb, midbrain; ob, olfactory bulb; pa, pharyngeal arches; sp, spinal cord. *$p < 0.05$; **$p < 0.01$; ***$p < 0.001$; n.s., not significant.

gene as a strong gene candidate for these diseases. In recent years, gene discovery has shifted from identifying pathogenic variants in genes for rare diseases to ultra-rare entities with only a handful of affected individuals. Indeed, this is supported by several recently uncovered leukodystrophy genes, in which only a few individuals were identified and published, including *EPRS1*, *POLR3K*, *RARS1*, *TMEM106B* (MIM: 613413), *CNP* (MIM:123830), and *NKX6-2* (MIM: 605955).[13,19,76–79] *LSM7*, which encodes a subunit of both the LSM1-7 and LSM2-8 complexes, has not previously been associated with human disease. However, other proteins involved in the processes of mRNA decay and splicing, the primary functions of the LSM1-7 and LSM2-8 complexes, respectively, have been implicated in a variety of diseases.[21,23,30,80–96] Cellular decay pathways play a critical role in regulating mRNA levels, and alterations in these pathways could be the principle factor underlying many diseases,[85–95,97,98] including neurological disorders.[83,84] Similarly, variants in genes encoding proteins involved in the various steps of the splicing reaction have also been linked to numerous neurodevelopmental and neurodegenerative disorders.[59,99–104] The identification of other individuals with biallelic variants in *LSM7* is needed to add with certainty this gene and the pathophysiological mechanisms of mRNA decay and splicing regulation to genes and categories of cellular dysfunction associated with leukodystrophies, genetic neurodevelopmental and/or neurodegenerative disorders.

Data and code availability

The clinical exomes are not publicly available. The variants generated during this study are available at ClinVar (gene variants; ClinVar: SCV001478394 and SCV001478886).

Supplemental information

Supplemental information can be found online at https://doi.org/10.1016/j.xhgg.2021.100034.

Acknowledgments

First and foremost, we would like to thank the individuals and their families for their participation. This study was supported by grants from the Canadian Institutes of Health Research (377869, 426534), Fondation Les Amis d'Elliot, Fondation le Tout pour Loo, and Réseau de Médicine Génétique Appliquée of the Fonds de Recherche du Québec – Santé (FRQS). This research was enabled in part by support provided by Compute Canada. A.D. was supported by the Canadian Institutes of Health Research (CIHR) Canadian Graduates Scholarships – Master's, the Fondation du Grand Défi Pierre Lavoie Master's Scholarship, and Heathy Brains for Healthy Lives Masters Fellowship. G.B. has received a Research Scholar Junior 1 award from the Fonds de Recherche du Québec - Santé (2012–2016) and the New Investigator Salary Award from the Canadian Institutes of Health Research (2017–2022). B.C. holds a Bell-Bombardier Research Chair awarded by the IRCM. We would also like to thank the McGill University and Genome Québec Innovation Center, the IRCM Molecular Biology and Functional Genomics Platform, and Denis Faubert, Josée Champagne, and Sylvain Tessier of the IRCM Proteomics Discovery Platform for their services.

Declaration of interests

Y.S. is an employee of GeneDx, Inc. J.L.B. reports being on the board of directors for wFluidx; stock ownership of Orchard Therapeutics; consulting for Bluebird, Calico, Denali, Enzyvant, Neurogene, and Passage Bio; and royalties from BioFire (spouse). G.B. reports speaker's honoraria from Genzyme (2013) and Actelion Pharmaceuticals (2013); being on the scientific advisory boards of Ionis (2019), Shire (2013), Actelion Pharmaceuticals (2011), and Santhera Pharmaceuticals (2011); research grant from Takeda; being on a site PI for studies sponsored by Takeda/Shire (2020-2021), Bluebird Bio (2019), Shire (2016), and Actelion Pharmaceuticals (2017); and consulting for Passage Bio. All other authors declare no competing interests.

Received: April 16, 2021
Accepted: April 28, 2021

Web resources

CHOPCHOP, http://chopchop.cbu.uib.no/
Compute Canada, https://www.computecanada.ca/
GenBank, https://www.ncbi.nlm.nih.gov/genbank/
GeneDx ClinVar submission page, https://www.ncbi.nlm.nih.gov/clinvar/submitters/26957
OMIM, https://omim.org/
PRALINE, https://www.ibi.vu.nl/programs/pralinewww/
PyMOL Molecular Graphics System, Version 2.0 Schrödinger, LLC, https://www.pymol.org/2/

References

1. Vanderver, A., Prust, M., Tonduti, D., Mochel, F., Hussey, H.M., Helman, G., Garbern, J., Eichler, F., Labauge, P., Aubourg, P., et al.; GLIA Consortium (2015). Case definition and classification of leukodystrophies and leukoencephalopathies. Mol. Genet. Metab. *114*, 494–500.
2. Parikh, S., Bernard, G., Leventer, R.J., van der Knaap, M.S., van Hove, J., Pizzino, A., McNeill, N.H., Helman, G., Simons, C., Schmidt, J.L., et al.; GLIA Consortium (2015). A clinical approach to the diagnosis of patients with leukodystrophies and genetic leukoencephelopathies. Mol. Genet. Metab. *114*, 501–515.
3. Ashrafi, M.R., and Tavasoli, A.R. (2017). Childhood leukodystrophies: A literature review of updates on new definitions, classification, diagnostic approach and management. Brain Dev. *39*, 369–385.
4. Schiffmann, R., and van der Knaap, M.S. (2009). Invited article: an MRI-based approach to the diagnosis of white matter disorders. Neurology *72*, 750–759.
5. Steenweg, M.E., Vanderver, A., Blaser, S., Bizzi, A., de Koning, T.J., Mancini, G.M., van Wieringen, W.N., Barkhof, F., Wolf, N.I., and van der Knaap, M.S. (2010). Magnetic resonance imaging pattern recognition in hypomyelinating disorders. Brain *133*, 2971–2982.
6. Bonkowsky, J.L., Nelson, C., Kingston, J.L., Filloux, F.M., Mundorff, M.B., and Srivastava, R. (2010). The burden of

inherited leukodystrophies in children. Neurology *75*, 718–725.
7. Adang, L.A., Sherbini, O., Ball, L., Bloom, M., Darbari, A., Amartino, H., DiVito, D., Eichler, F., Escolar, M., Evans, S.H., et al.; Global Leukodystrophy Initiative (GLIA) Consortium (2017). Revised consensus statement on the preventive and symptomatic care of patients with leukodystrophies. Mol. Genet. Metab. *122*, 18–32.
8. van der Knaap, M.S., and Bugiani, M. (2017). Leukodystrophies: a proposed classification system based on pathological changes and pathogenetic mechanisms. Acta Neuropathol. *134*, 351–382.
9. Vanderver, A., Simons, C., Helman, G., Crawford, J., Wolf, N.I., Bernard, G., Pizzino, A., Schmidt, J.L., Takanohashi, A., Miller, D., et al.; Leukodystrophy Study Group (2016). Whole exome sequencing in patients with white matter abnormalities. Ann. Neurol. *79*, 1031–1037.
10. Kevelam, S.H., Steenweg, M.E., Srivastava, S., Helman, G., Naidu, S., Schiffmann, R., Blaser, S., Vanderver, A., Wolf, N.I., and van der Knaap, M.S. (2016). Update on Leukodystrophies: A Historical Perspective and Adapted Definition. Neuropediatrics *47*, 349–354.
11. Boycott, K.M., Vanstone, M.R., Bulman, D.E., and MacKenzie, A.E. (2013). Rare-disease genetics in the era of next-generation sequencing: discovery to translation. Nat. Rev. Genet. *14*, 681–691.
12. Sawyer, S.L., Hartley, T., Dyment, D.A., Beaulieu, C.L., Schwartzentruber, J., Smith, A., Bedford, H.M., Bernard, G., Bernier, F.P., Brais, B., et al.; FORGE Canada Consortium; and Care4Rare Canada Consortium (2016). Utility of whole-exome sequencing for those near the end of the diagnostic odyssey: time to address gaps in care. Clin. Genet. *89*, 275–284.
13. Mendes, M.I., Gutierrez Salazar, M., Guerrero, K., Thiffault, I., Salomons, G.S., Gauquelin, L., Tran, L.T., Forget, D., Gauthier, M.S., Waisfisz, Q., et al. (2018). Bi-allelic Mutations in EPRS, Encoding the Glutamyl-Prolyl-Aminoacyl-tRNA Synthetase, Cause a Hypomyelinating Leukodystrophy. Am. J. Hum. Genet. *102*, 676–684.
14. Rezaei, Z., Hosseinpour, S., Ashrafi, M.R., Mahdieh, N., Alizadeh, H., Mohammadpour, M., Khosroshahi, N., Amanat, M., and Tavasoli, A.R. (2019). Hypomyelinating Leukodystrophy with Spinal Cord Involvement Caused by a Novel Variant in RARS: Report of Two Unrelated Patients. Neuropediatrics *50*, 130–134.
15. Friedman, J., Smith, D.E., Issa, M.Y., Stanley, V., Wang, R., Mendes, M.I., Wright, M.S., Wigby, K., Hildreth, A., Crawford, J.R., et al. (2019). Biallelic mutations in valyl-tRNA synthetase gene VARS are associated with a progressive neurodevelopmental epileptic encephalopathy. Nat. Commun. *10*, 707.
16. Thiffault, I., Wolf, N.I., Forget, D., Guerrero, K., Tran, L.T., Choquet, K., Lavallée-Adam, M., Poitras, C., Brais, B., Yoon, G., et al. (2015). Recessive mutations in POLR1C cause a leukodystrophy by impairing biogenesis of RNA polymerase III. Nat. Commun. *6*, 7623.
17. Bernard, G., Chouery, E., Putorti, M.L., Tétreault, M., Takanohashi, A., Carosso, G., Clément, I., Boespflug-Tanguy, O., Rodriguez, D., Delague, V., et al. (2011). Mutations of POLR3A encoding a catalytic subunit of RNA polymerase Pol III cause a recessive hypomyelinating leukodystrophy. Am. J. Hum. Genet. *89*, 415–423.
18. Tétreault, M., Choquet, K., Orcesi, S., Tonduti, D., Balottin, U., Teichmann, M., Fribourg, S., Schiffmann, R., Brais, B., Vanderver, A., and Bernard, G. (2011). Recessive mutations in POLR3B, encoding the second largest subunit of Pol III, cause a rare hypomyelinating leukodystrophy. Am. J. Hum. Genet. *89*, 652–655.
19. Dorboz, I., Dumay-Odelot, H., Boussaid, K., Bouyacoub, Y., Barreau, P., Samaan, S., Jmel, H., Eymard-Pierre, E., Cances, C., Bar, C., et al. (2018). Mutation in *POLR3K* causes hypomyelinating leukodystrophy and abnormal ribosomal RNA regulation. Neurol. Genet. *4*, e289.
20. Tharun, S. (2009). Roles of eukaryotic Lsm proteins in the regulation of mRNA function. Int. Rev. Cell Mol. Biol. *272*, 149–189.
21. Tharun, S. (2009). Lsm1-7-Pat1 complex: a link between 3′ and 5′-ends in mRNA decay? RNA Biol. *6*, 228–232.
22. Beggs, J.D. (2005). Lsm proteins and RNA processing. Biochem. Soc. Trans. *33*, 433–438.
23. Kufel, J., Bousquet-Antonelli, C., Beggs, J.D., and Tollervey, D. (2004). Nuclear pre-mRNA decapping and 5′ degradation in yeast require the Lsm2-8p complex. Mol. Cell. Biol. *24*, 9646–9657.
24. Sharif, H., and Conti, E. (2013). Architecture of the Lsm1-7-Pat1 complex: a conserved assembly in eukaryotic mRNA turnover. Cell Rep. *5*, 283–291.
25. Chowdhury, A., Mukhopadhyay, J., and Tharun, S. (2007). The decapping activator Lsm1p-7p-Pat1p complex has the intrinsic ability to distinguish between oligoadenylated and polyadenylated RNAs. RNA *13*, 998–1016.
26. Wu, D., Muhlrad, D., Bowler, M.W., Jiang, S., Liu, Z., Parker, R., and Song, H. (2014). Lsm2 and Lsm3 bridge the interaction of the Lsm1-7 complex with Pat1 for decapping activation. Cell Res. *24*, 233–246.
27. Friesen, W.J., and Dreyfuss, G. (2000). Specific sequences of the Sm and Sm-like (Lsm) proteins mediate their interaction with the spinal muscular atrophy disease gene product (SMN). J. Biol. Chem. *275*, 26370–26375.
28. Will, C.L., and Lührmann, R. (2011). Spliceosome structure and function. Cold Spring Harb. Perspect. Biol. *3*, a003707.
29. Chen, W., and Moore, M.J. (2015). Spliceosomes. Curr. Biol. *25*, R181–R183.
30. Verdone, L., Galardi, S., Page, D., and Beggs, J.D. (2004). Lsm proteins promote regeneration of pre-mRNA splicing activity. Curr. Biol. *14*, 1487–1491.
31. Wilusz, C.J., and Wilusz, J. (2013). Lsm proteins and Hfq: Life at the 3′ end. RNA Biol. *10*, 592–601.
32. Retterer, K., Juusola, J., Cho, M.T., Vitazka, P., Millan, F., Gibellini, F., Vertino-Bell, A., Smaoui, N., Neidich, J., Monaghan, K.G., et al. (2016). Clinical application of whole-exome sequencing across clinical indications. Genet. Med. *18*, 696–704.
33. Richards, S., Aziz, N., Bale, S., Bick, D., Das, S., Gastier-Foster, J., Grody, W.W., Hegde, M., Lyon, E., Spector, E., et al.; ACMG Laboratory Quality Assurance Committee (2015). Standards and guidelines for the interpretation of sequence variants: a joint consensus recommendation of the American College of Medical Genetics and Genomics and the Association for Molecular Pathology. Genet. Med. *17*, 405–424.
34. Sobreira, N., Schiettecatte, F., Boehm, C., Valle, D., and Hamosh, A. (2015). New tools for Mendelian disease gene identification: PhenoDB variant analysis module; and

GeneMatcher, a web-based tool for linking investigators with an interest in the same gene. Hum. Mutat. *36*, 425–431.

35. Sobreira, N., Schiettecatte, F., Valle, D., and Hamosh, A. (2015). GeneMatcher: a matching tool for connecting investigators with an interest in the same gene. Hum. Mutat. *36*, 928–930.
36. Monies, D., Abouelhoda, M., Assoum, M., Moghrabi, N., Rafiullah, R., Almontashiri, N., Alowain, M., Alzaidan, H., Alsayed, M., Subhani, S., et al. (2019). Lessons Learned from Large-Scale, First-Tier Clinical Exome Sequencing in a Highly Consanguineous Population. Am. J. Hum. Genet. *105*, 879.
37. Lek, M., Karczewski, K.J., Minikel, E.V., Samocha, K.E., Banks, E., Fennell, T., O'Donnell-Luria, A.H., Ware, J.S., Hill, A.J., Cummings, B.B., et al.; Exome Aggregation Consortium (2016). Analysis of protein-coding genetic variation in 60,706 humans. Nature *536*, 285–291.
38. Ng, P.C., and Henikoff, S. (2003). SIFT: Predicting amino acid changes that affect protein function. Nucleic Acids Res. *31*, 3812–3814.
39. Choi, Y., and Chan, A.P. (2015). PROVEAN web server: a tool to predict the functional effect of amino acid substitutions and indels. Bioinformatics *31*, 2745–2747.
40. Kircher, M., Witten, D.M., Jain, P., O'Roak, B.J., Cooper, G.M., and Shendure, J. (2014). A general framework for estimating the relative pathogenicity of human genetic variants. Nat. Genet. *46*, 310–315.
41. Rentzsch, P., Witten, D., Cooper, G.M., Shendure, J., and Kircher, M. (2019). CADD: predicting the deleteriousness of variants throughout the human genome. Nucleic Acids Res. *47* (D1), D886–D894.
42. Schwarz, J.M., Cooper, D.N., Schuelke, M., and Seelow, D. (2014). MutationTaster2: mutation prediction for the deep-sequencing age. Nat. Methods *11*, 361–362.
43. Taylor, S., Wakem, M., Dijkman, G., Alsarraj, M., and Nguyen, M. (2010). A practical approach to RT-qPCR-Publishing data that conform to the MIQE guidelines. Methods *50*, S1–S5.
44. Taylor, S.C., and Mrkusich, E.M. (2014). The state of RT-quantitative PCR: firsthand observations of implementation of minimum information for the publication of quantitative real-time PCR experiments (MIQE). J. Mol. Microbiol. Biotechnol. *24*, 46–52.
45. Zhou, L., Hang, J., Zhou, Y., Wan, R., Lu, G., Yin, P., Yan, C., and Shi, Y. (2014). Crystal structures of the Lsm complex bound to the 3′ end sequence of U6 small nuclear RNA. Nature *506*, 116–120.
46. Chen, G.I., and Gingras, A.C. (2007). Affinity-purification mass spectrometry (AP-MS) of serine/threonine phosphatases. Methods *42*, 298–305.
47. Mellacheruvu, D., Wright, Z., Couzens, A.L., Lambert, J.P., St-Denis, N.A., Li, T., Miteva, Y.V., Hauri, S., Sardiu, M.E., Low, T.Y., et al. (2013). The CRAPome: a contaminant repository for affinity purification-mass spectrometry data. Nat. Methods *10*, 730–736.
48. Cox, J., and Mann, M. (2008). MaxQuant enables high peptide identification rates, individualized p.p.b.-range mass accuracies and proteome-wide protein quantification. Nat. Biotechnol. *26*, 1367–1372.
49. Cox, J., Michalski, A., and Mann, M. (2011). Software lock mass by two-dimensional minimization of peptide mass errors. J. Am. Soc. Mass Spectrom. *22*, 1373–1380.
50. Cox, J., Hein, M.Y., Luber, C.A., Paron, I., Nagaraj, N., and Mann, M. (2014). Accurate proteome-wide label-free quantification by delayed normalization and maximal peptide ratio extraction, termed MaxLFQ. Mol. Cell. Proteomics *13*, 2513–2526.
51. Schaab, C., Geiger, T., Stoehr, G., Cox, J., and Mann, M. (2012). Analysis of high accuracy, quantitative proteomics data in the MaxQB database. Mol. Cell Proteomics *11*, M111.014068.
52. Tyanova, S., Temu, T., Carlson, A., Sinitcyn, P., Mann, M., and Cox, J. (2015). Visualization of LC-MS/MS proteomics data in MaxQuant. Proteomics *15*, 1453–1456.
53. Tyanova, S., Temu, T., and Cox, J. (2016). The MaxQuant computational platform for mass spectrometry-based shotgun proteomics. Nat. Protoc. *11*, 2301–2319.
54. Tyanova, S., Temu, T., Sinitcyn, P., Carlson, A., Hein, M.Y., Geiger, T., Mann, M., and Cox, J. (2016). The Perseus computational platform for comprehensive analysis of (prote)omics data. Nat. Methods *13*, 731–740.
55. Rudolph, J.D., and Cox, J. (2019). A Network Module for the Perseus Software for Computational Proteomics Facilitates Proteome Interaction Graph Analysis. J. Proteome Res. *18*, 2052–2064.
56. Tyanova, S., Albrechtsen, R., Kronqvist, P., Cox, J., Mann, M., and Geiger, T. (2016). Proteomic maps of breast cancer subtypes. Nat. Commun. *7*, 10259.
57. Cox, J., and Mann, M. (2012). 1D and 2D annotation enrichment: a statistical method integrating quantitative proteomics with complementary high-throughput data. BMC Bioinformatics *13* (*Suppl 16*), S12.
58. Choquet, K., Pinard, M., Yang, S., Moir, R.D., Poitras, C., Dicaire, M.J., Sgarioto, N., Larivière, R., Kleinman, C.L., Willis, I.M., et al. (2019). The leukodystrophy mutation Polr3b R103H causes homozygote mouse embryonic lethality and impairs RNA polymerase III biogenesis. Mol. Brain *12*, 59.
59. Vazquez-Arango, P., and O'Reilly, D. (2018). Variant snRNPs: New players within the spliceosome system. RNA Biol. *15*, 17–25.
60. Matera, A.G., and Wang, Z. (2014). A day in the life of the spliceosome. Nat. Rev. Mol. Cell Biol. *15*, 108–121.
61. Didychuk, A.L., Butcher, S.E., and Brow, D.A. (2018). The life of U6 small nuclear RNA, from cradle to grave. RNA *24*, 437–460.
62. Vindry, C., Marnef, A., Broomhead, H., Twyffels, L., Ozgur, S., Stoecklin, G., Llorian, M., Smith, C.W., Mata, J., Weil, D., and Standart, N. (2017). Dual RNA Processing Roles of Pat1b via Cytoplasmic Lsm1-7 and Nuclear Lsm2-8 Complexes. Cell Rep. *20*, 1187–1200.
63. Sabarinathan, R., Tafer, H., Seemann, S.E., Hofacker, I.L., Stadler, P.F., and Gorodkin, J. (2013). RNAsnp: efficient detection of local RNA secondary structure changes induced by SNPs. Hum. Mutat. *34*, 546–556.
64. Sharma, Y., Miladi, M., Dukare, S., Boulay, K., Caudron-Herger, M., Groß, M., Backofen, R., and Diederichs, S. (2019). A pan-cancer analysis of synonymous mutations. Nat. Commun. *10*, 2569.
65. Salari, R., Kimchi-Sarfaty, C., Gottesman, M.M., and Przytycka, T.M. (2013). Sensitive measurement of single-nucleotide polymorphism-induced changes of RNA conformation: application to disease studies. Nucleic Acids Res. *41*, 44–53.
66. Thisse, C., and Thisse, B. (2008). High-resolution in situ hybridization to whole-mount zebrafish embryos. Nat. Protoc. *3*, 59–69.

67. Bonkowsky, J.L., Wang, X., Fujimoto, E., Lee, J.E., Chien, C.B., and Dorsky, R.I. (2008). Domain-specific regulation of foxP2 CNS expression by lef1. BMC Dev. Biol. *8*, 103.
68. Lambert, A.M., Bonkowsky, J.L., and Masino, M.A. (2012). The conserved dopaminergic diencephalospinal tract mediates vertebrate locomotor development in zebrafish larvae. J. Neurosci. *32*, 13488–13500.
69. Minnerop, M., Kurzwelly, D., Wagner, H., Soehn, A.S., Reichbauer, J., Tao, F., Rattay, T.W., Peitz, M., Rehbach, K., Giorgetti, A., et al. (2017). Hypomorphic mutations in POLR3A are a frequent cause of sporadic and recessive spastic ataxia. Brain *140*, 1561–1578.
70. Harting, I., Al-Saady, M., Krägeloh-Mann, I., Bley, A., Hempel, M., Bierhals, T., Karch, S., Moog, U., Bernard, G., Huntsman, R., et al. (2020). POLR3A variants with striatal involvement and extrapyramidal movement disorder. Neurogenetics *21*, 121–133.
71. Hiraide, T., Kubota, K., Kono, Y., Watanabe, S., Matsubayashi, T., Nakashima, M., Kaname, T., Fukao, T., Shimozawa, N., Ogata, T., and Saitsu, H. (2020). POLR3A variants in striatal involvement without diffuse hypomyelination. Brain Dev. *42*, 363–368.
72. Perrier, S., Gauquelin, L., Fallet-Bianco, C., Dishop, M.K., Michell-Robinson, M.A., Tran, L.T., Guerrero, K., Darbelli, L., Srour, M., Petrecca, K., et al. (2020). Expanding the phenotypic and molecular spectrum of RNA polymerase III-related leukodystrophy. Neurol. Genet. *6*, e425.
73. Wu, S., Bai, Z., Dong, X., Yang, D., Chen, H., Hua, J., Zhou, L., and Lv, H. (2019). Novel mutations of the POLR3A gene caused POLR3-related leukodystrophy in a Chinese family: a case report. BMC Pediatr. *19*, 289.
74. Gauquelin, L., Cayami, F.K., Sztriha, L., Yoon, G., Tran, L.T., Guerrero, K., Hocke, F., van Spaendonk, R.M.L., Fung, E.L., D'Arrigo, S., et al.; DDD Study (2019). Clinical spectrum of POLR3-related leukodystrophy caused by biallelic *POLR1C* pathogenic variants. Neurol. Genet. *5*, e369.
75. Landau, D., Cohen, D., Shalev, H., Pinsk, V., Yerushalmi, B., Zeigler, M., and Birk, O.S. (2004). A novel mutation in the SLC17A5 gene causing both severe and mild phenotypes of free sialic acid storage disease in one inbred Bedouin kindred. Mol. Genet. Metab. *82*, 167–172.
76. Ito, Y., Hartley, T., Baird, S., Venkateswaran, S., Simons, C., Wolf, N.I., Boycott, K.M., Dyment, D.A., and Kernohan, K.D. (2018). Lysosomal dysfunction in *TMEM106B* hypomyelinating leukodystrophy. Neurol. Genet. *4*, e288.
77. Wolf, N.I., Salomons, G.S., Rodenburg, R.J., Pouwels, P.J., Schieving, J.H., Derks, T.G., Fock, J.M., Rump, P., van Beek, D.M., van der Knaap, M.S., and Waisfisz, Q. (2014). Mutations in RARS cause hypomyelination. Ann. Neurol. *76*, 134–139.
78. Al-Abdi, L., Al Murshedi, F., Elmanzalawy, A., Al Habsi, A., Helaby, R., Ganesh, A., Ibrahim, N., Patel, N., and Alkuraya, F.S. (2020). CNP deficiency causes severe hypomyelinating leukodystrophy in humans. Hum. Genet. *139*, 615–622.
79. Chelban, V., Patel, N., Vandrovcova, J., Zanetti, M.N., Lynch, D.S., Ryten, M., Botía, J.A., Bello, O., Tribollet, E., Efthymiou, S., et al.; SYNAPSE Study Group (2017). Mutations in NKX6-2 Cause Progressive Spastic Ataxia and Hypomyelination. Am. J. Hum. Genet. *100*, 969–977.
80. Kufel, J., Allmang, C., Petfalski, E., Beggs, J., and Tollervey, D. (2003). Lsm Proteins are required for normal processing and stability of ribosomal RNAs. J. Biol. Chem. *278*, 2147–2156.
81. Ingelfinger, D., Arndt-Jovin, D.J., Lührmann, R., and Achsel, T. (2002). The human LSm1-7 proteins colocalize with the mRNA-degrading enzymes Dcp1/2 and Xrnl in distinct cytoplasmic foci. RNA *8*, 1489–1501.
82. He, W., and Parker, R. (2001). The yeast cytoplasmic LsmI/Pat1p complex protects mRNA 3′ termini from partial degradation. Genetics *158*, 1445–1455.
83. Hollams, E.M., Giles, K.M., Thomson, A.M., and Leedman, P.J. (2002). MRNA stability and the control of gene expression: implications for human disease. Neurochem. Res. *27*, 957–980.
84. Linder, B., Fischer, U., and Gehring, N.H. (2015). mRNA metabolism and neuronal disease. FEBS Lett. *589*, 1598–1606.
85. Vlasova-St Louis, I., Dickson, A.M., Bohjanen, P.R., and Wilusz, C.J. (2013). CELFish ways to modulate mRNA decay. Biochim. Biophys. Acta *1829*, 695–707.
86. Eberhardt, W., Doller, A., Akool, S., and Pfeilschifter, J. (2007). Modulation of mRNA stability as a novel therapeutic approach. Pharmacol. Ther. *114*, 56–73.
87. Schoenberg, D.R., and Maquat, L.E. (2012). Regulation of cytoplasmic mRNA decay. Nat. Rev. Genet. *13*, 246–259.
88. Cheneval, D., Kastelic, T., Fuerst, P., and Parker, C.N. (2010). A review of methods to monitor the modulation of mRNA stability: a novel approach to drug discovery and therapeutic intervention. J. Biomol. Screen. *15*, 609–622.
89. Anderson, P. (2010). Post-transcriptional regulons coordinate the initiation and resolution of inflammation. Nat. Rev. Immunol. *10*, 24–35.
90. Frischmeyer, P.A., and Dietz, H.C. (1999). Nonsense-mediated mRNA decay in health and disease. Hum. Mol. Genet. *8*, 1893–1900.
91. Benjamin, D., and Moroni, C. (2007). mRNA stability and cancer: an emerging link? Expert Opin. Biol. Ther. *7*, 1515–1529.
92. Khajavi, M., Inoue, K., and Lupski, J.R. (2006). Nonsense-mediated mRNA decay modulates clinical outcome of genetic disease. Eur. J. Hum. Genet. *14*, 1074–1081.
93. Miller, J.N., and Pearce, D.A. (2014). Nonsense-mediated decay in genetic disease: friend or foe? Mutat. Res. Rev. Mutat. Res. *762*, 52–64.
94. Pashler, A.L., Towler, B.P., Jones, C.I., and Newbury, S.F. (2016). The roles of the exoribonucleases DIS3L2 and XRN1 in human disease. Biochem. Soc. Trans. *44*, 1377–1384.
95. Morita, M., Siddiqui, N., Katsumura, S., Rouya, C., Larsson, O., Nagashima, T., Hekmatnejad, B., Takahashi, A., Kiyonari, H., Zang, M., et al. (2019). Hepatic posttranscriptional network comprised of CCR4-NOT deadenylase and FGF21 maintains systemic metabolic homeostasis. Proc. Natl. Acad. Sci. USA *116*, 7973–7981.
96. Sveen, A., Kilpinen, S., Ruusulehto, A., Lothe, R.A., and Skotheim, R.I. (2016). Aberrant RNA splicing in cancer; expression changes and driver mutations of splicing factor genes. Oncogene *35*, 2413–2427.
97. Weskamp, K., and Barmada, S.J. (2018). RNA Degradation in Neurodegenerative Disease. Adv. Neurobiol. *20*, 103–142.
98. Kapur, M., Monaghan, C.E., and Ackerman, S.L. (2017). Regulation of mRNA Translation in Neurons-A Matter of Life and Death. Neuron *96*, 616–637.
99. Padgett, R.A. (2012). New connections between splicing and human disease. Trends Genet. *28*, 147–154.

100. Faustino, N.A., and Cooper, T.A. (2003). Pre-mRNA splicing and human disease. Genes Dev. *17*, 419–437.
101. Jutzi, D., Akinyi, M.V., Mechtersheimer, J., Frilander, M.J., and Ruepp, M.D. (2018). The emerging role of minor intron splicing in neurological disorders. Cell Stress *2*, 40–54.
102. Pasternack, S.M., Refke, M., Paknia, E., Hennies, H.C., Franz, T., Schäfer, N., Fryer, A., van Steensel, M., Sweeney, E., Just, M., et al. (2013). Mutations in SNRPE, which encodes a core protein of the spliceosome, cause autosomal-dominant hypotrichosis simplex. Am. J. Hum. Genet. *92*, 81–87.
103. Lynch, D.C., Revil, T., Schwartzentruber, J., Bhoj, E.J., Innes, A.M., Lamont, R.E., Lemire, E.G., Chodirker, B.N., Taylor, J.P., Zackai, E.H., et al.; Care4Rare Canada (2014). Disrupted auto-regulation of the spliceosomal gene SNRPB causes cerebro-costo-mandibular syndrome. Nat. Commun. *5*, 4483.
104. Bacrot, S., Doyard, M., Huber, C., Alibeu, O., Feldhahn, N., Lehalle, D., Lacombe, D., Marlin, S., Nitschke, P., Petit, F., et al. (2015). Mutations in SNRPB, encoding components of the core splicing machinery, cause cerebro-costo-mandibular syndrome. Hum. Mutat. *36*, 187–190.

HGGA, Volume *2*

Supplemental information

Variants in *LSM7* impair LSM complexes assembly, neurodevelopment in zebrafish and may be associated with an ultra-rare neurological disease

Alexa Derksen, Hung-Yu Shih, Diane Forget, Lama Darbelli, Luan T. Tran, Christian Poitras, Kether Guerrero, Sundaresan Tharun, Fowzan S. Alkuraya, Wesam I. Kurdi, Cam-Tu Emilie Nguyen, Anne-Marie Laberge, Yue Si, Marie-Soleil Gauthier, Joshua L. Bonkowsky, Benoit Coulombe, and Geneviève Bernard

Supplemental Figures:

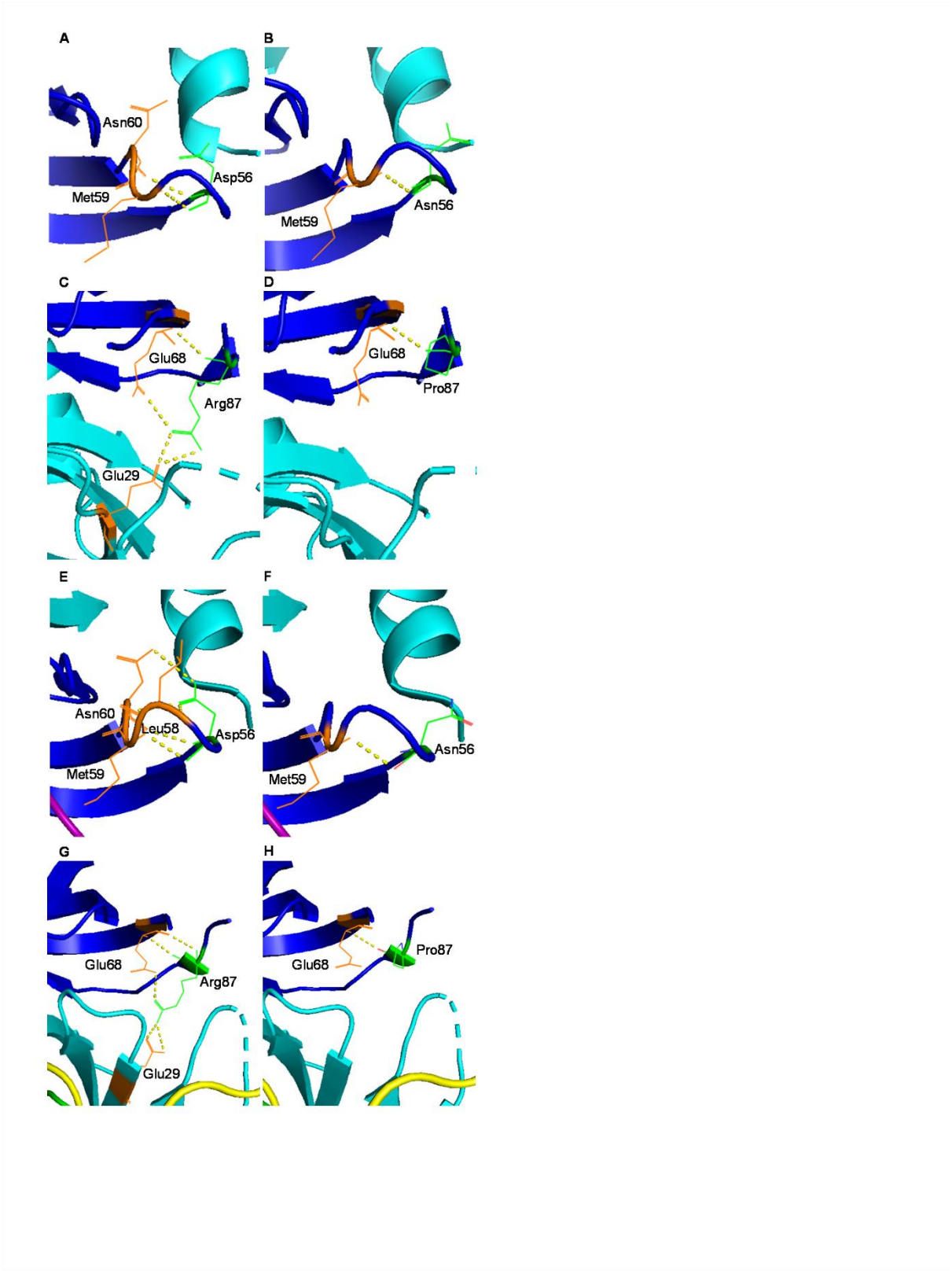

Figure S1. 3D representation of predicted mutational impact on LSM1-7 and LSM2-8 structures created with PyMOL.

(A-D) Pair-wise comparisons between the wild-type (left) and mutant (right) residues in LSM1-7 complex.

(A) Asp56 residue on yeast Lsm7 has polar contacts with Lsm7 residues Met59 and Asn60 in LSM1-7 complex.

(B) Asn56 mutant residue on yeast Lsm7 only has polar contacts with the Lsm7 residue Met59 in the LSM1-7 complex and has lost its interaction with the Asn60 residue.

(C) Arg87 residue on yeast Lsm7 has polar contacts with Lsm7 residue Glu68 and Lsm5 residue Glu29 in the LSM1-7 complex.

(D) Pro87 mutant residue on yeast Lsm7 only has polar contacts with Lsm7 residue Glu68 in the LSM1-7 complex and has lost its interaction with the Glu29 residue of Lsm5.

(E-H) Pair-wise comparisons between the wild-type (left) and mutant (right) residues in LSM2-8 complex.

(E) Asp56 residue on yeast Lsm7 has polar contacts with Lsm7 residues Leu58, Met59 and Asn60 in the LSM2-8 complex.

(F) Asn56 mutant residue on yeast Lsm7 only has polar contacts with Lsm7 residue Met59 in the LSM2-8 complex and has lost its interaction with Met59 and Asn60.

(G) Arg87 residue on yeast Lsm7 has polar contacts with Lsm7 residue Glu68 and Lsm5 residue Glu29 in the LSM2-8 complex.

(H) Pro87 mutant residue on yeast Lsm7 only has polar contacts with Lsm7 residue Glu68 in the LSM2-8 complex and has lost its interaction with the Lsm5 residue Glu29.

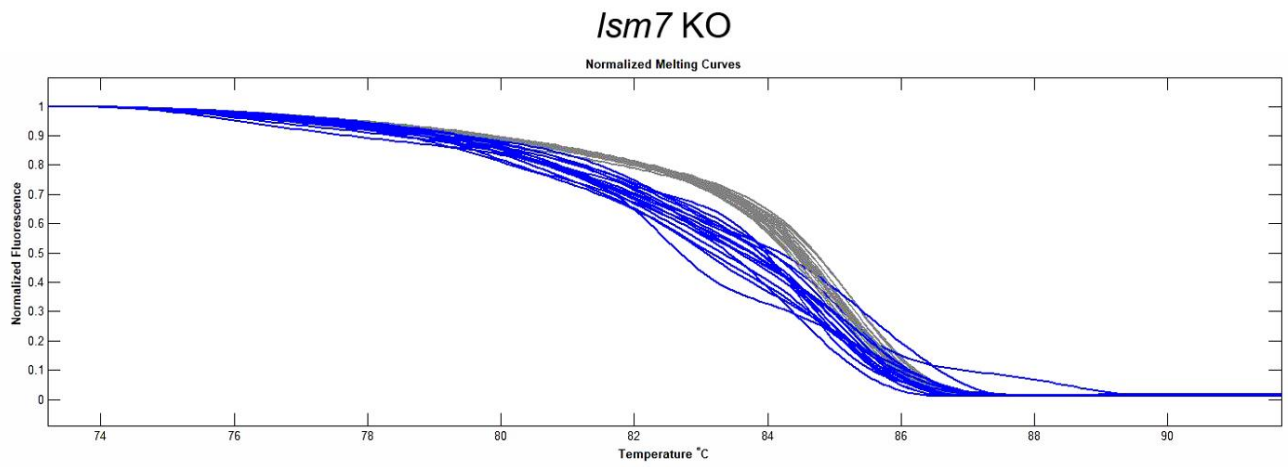

Figure S2. Lsm7 sgRNA could efficiently induce insertion and/or deletion formation of lsm7 loci.

HRMA analysis of wild-type embryos and Lsm7-Crispants. Gray curves, wild-type; blue curves, Lsm7-Crispants. X-axis, melt temperature (˚C); y-axis, normalized change in fluorescence with temperature.

Supplemental Table:

Table S1. *In silico* analysis using damage prediction algorithms and highest minor allele frequency in GnomAD

Variant	Mutation Taster	SIFT	CADD	Provean	PolyPhen2	MAF (GnomAD)
c.121G>A (p.Asp41Asn)	Disease Causing	Deleterious	Deleterious	Deleterious	Probably Damaging	3.87e-5
c.206G>C (p.Arg69Pro)	Disease Causing	Deleterious	Deleterious	Deleterious	Probably Damaging	Absent

Supplemental Material and Methods:

Affected individual ascertainment

Experiments involving human participants or data were conducted in compliance with all relevant ethical regulations. Informed consent was obtained from all participants. Approval for human subjects' research was obtained at the McGill University Health Centre Research Research Ethics Board (project number PED-11-105, 2019-4972). Clinical brain MRIs were obtained for individual 1 and longitudinal clinical assessment performed in order to determine disease course. Saliva samples were collected for DNA isolation from individual 1 and his mother and father. A dermal skin punch was also obtained from individual 1 after informed consent and was cultured in 10% fetal bovine serum and DMEM to obtain low passage primary fibroblasts. Consent for clinical next generation sequencing of both parents of individual 2 was obtained at the King Faisal Specialist Hospital and Research Centre in Riyadh, Saudi Arabia.

Whole exome sequencing and variant identification

Clinical whole exome sequencing was performed on affected individual 1, as a trio with biological parents by GeneDx. The exonic regions and flanking splice junctions of the genome were captured using a proprietary system developed by GeneDx and sequenced by massive parallel (NextGen) sequencing on an Illumina system with 100bp or greater paired-end reads. Reads were aligned to human genome build GRCh37/UCSC hg 19 and analyzed for sequence variants using a custom developed analysis tool (Xome Analyzer). Additional sequencing technology and variant interpretation protocols have been previously described.[1] Capillary sequencing or

another appropriate method was used to confirm all potentially pathogenic variants identified in individual 1 and their relative samples. The general assertion criteria for variant classification are publicly available on GeneDx ClinVar submission page. A second analysis of the sequence variants was conducted in-house at the MyeliNeuroGene lab of the Research Institute of the McGill University Health Centre. Sequence variants were prioritized using the standard and guidelines for interpretation set out by the American College of Medical Genetics (ACMG).[2] Clinical whole exome sequencing was performed on the parents of individual 2 as previously described.[3]

Cell culture

Fibroblasts from individual 1 and two age- and sex-matched controls were grown in DMEM supplemented with 10% fetal bovine serum and maintained at 37°C and 5% CO_2. Each cell line was expanded and harvested at similar passages at least three consecutive times for use in molecular experiments. HEK293T cells were grown in DMEM media supplemented with 10% fetal bovine serum, 2mM glutamine and 1% penicillin-streptomycin and maintained at 37°C and 5% CO_2.

RT-qPCR

RNA was extracted from fibroblasts using TRIzol reagent according to manufacturer's instructions (Invitrogen). For each sample, 1µg of total RNA was reverse transcribed using M-MLV reverse transcriptase (Promega) and random hexamers (Invitrogen) according to manufacturer's protocol (Promega). Primers for RT-qPCR were designed, and efficiency tested according to the MIQE guidelines.[4, 5] Primers were as follows:

LSM7 forward 5'-GAAGCCAGTGGAATCCTGAAGG-3'; *LSM7* reverse: 5'-CCTCCGTGAGCTTGTACTGG-3'; *U6 snRNA* forward: 5'-CTCGCTTCGGCAGCACA-3'; *U6 snRNA* reverse: 5'-AACGCTTCACGAATTTGCGT-3'; *RPL30* forward: 5'-AAGGCAGGAAGATGGTGGCC-3'; *RPL30* reverse: 5'-GAGTCTGCTTGTACCCCAGGAC-3'; and *SDHA* forward: 5'-CAGCATGTGTTACCAAGCTG-3'; *SDHA* reverse: 5'-GGTGTCGTAGAAATGCCAAC-3'. Reverse transcription was performed in triplicate with a 1:4 dilution of cDNA using SsoAdvanced Universal SYBR Green Supermix (Biorad) on the Roche LightCycler 96. All data were normalized to *SDHA* or *RPL30* using the ΔΔCt method in accordance with the MIQE guidelines.[4, 5]

Western blot

Total protein was extracted from fibroblasts in ice cold RIPA buffer with protease inhibitors (Roche) and spun down for 20 minutes at maximum speed. Protein concentration was determined using the Bradford protein assay in cuvettes according to manufacturer's instructions (Biorad). 30ug of protein were separated on a 15% SDS-polyacrylamide gel and transferred to a nitrocellulose membrane using the Bio-Rad Trans-Blot Turbo Transfer System. The membranes were first blocked with 1X TBST with 5% w/v non-fat dry milk and then probed with primary antibodies against LSM7 (Abcam 241656, dilution 1:10,000) and against beta-tubulin (Abcam 6046, dilution 1:20,000) diluted in primary antibody buffer overnight at 4℃. The next day, a secondary polyclonal goat-anti rabbit IgG (H+L) (Novus biologicals, 1:5,000) antibody was used in 5% w/v non-fat milk in TBST and membranes were subsequently

visualized with Amersham ECL Western Blot Detecting Reagent according to manufacturer's protocol (GE Life Sciences).

Construction of Lsm1-7 and Lsm2-8 structural models

Structural models of the wild-type and mutant yeast Lsm1-7 (PDB ID 4M75)[6] and Lsm2-8 complexes (PDB ID 4M77)[6] were generated using PyMOL Molecular Graphics System, Version 2.0 Schrödinger, LLC.

Protein affinity purification coupled to mass spectrometry

Plasmids for 3xFLAG-tagged LSM7 wild-type and the two mutants (p.Asp41Asn and p.Arg69Pro) were generated using the p3xFLAG-CMV-14 plasmid (Sigma). 0.4ug of the plasmids were transfected into HEK293 cells seeded at 80% confluence in 6-well plates using jetPRIME DNA transfection reagent kit according to manufacturer's protocol (Polyplus-Transfection). The HEK293 cells were maintained in culture in DMEM media supplemented with 10% fetal bovine serum, 1% penicillin-streptomycin and 1% L-glutamine. Forty-eight hours after transfection, protein lysates were collected using a gentle lysis buffer to preserve protein-protein interactions and quantified in a 96-well plate using Bradford Reagent according to manufacturer's protocol (LifeTechnologies). Equal amounts of protein were purified using FLAG M2 magnetic beads according to standard procedures in 4 independent replicate experiments.[7, 8] The protein extracts were dried down in a speed-vac before being resolubilized and digested with trypsin. The tryptic peptides were then purified and identified using tandem mass spectrometry (LC-MS/MS) with an HPLC system coupled to Orbitrap fusion mass spectrometer

(Thermo Scientific) through a Nanospray Flex Ion Source. Protein database searching was performed using MaxQuant version 1.6.10.43[9-14] against the SwissProt human protein database downloaded on 4 April 2019. Default MaxQuant parameters were modified as follows: trypsin was used as the digestion enzyme, LFQ computation and "Match between runs" were activated. Known AP-MS protein contaminants including keratins were excluded. Protein intensities were analysed using Perseus version 1.6.10.43.[15-18] Proteins marked by MaxQuant as being "Only identified by site" and "Reverse" were excluded. Proteins not present in at least 3 out of 4 replicates of WT, p.Asp41Asn, or p.Arg69Pro were excluded. Missing LFQ values were replaced by normally distributed values with a mean downshifted by 1.8 and a standard deviation of 0.3 times the non-missing values. WT, p.Asp41Asn, and p.Arg69Pro proteins were compared against FLAG empty vector control samples and were labeled as high-confidence interactors when their adjusted p-values were under 0.05 and their intensity ratio over 2. P-values were corrected with a permutation-based approach using an s0 correction factor of 0.1 with 10,000 iterations.[19] A Student's *t*-test was performed between p.Asp41Asn and p.Arg69Pro against the WT samples. For the generation of the heatmap, log2 ratios were computed between the means of the WT, p.Asp41Asn, and p.Arg69Pro against WT for known interactors of LSM7.

Zebrafish ethics statement

Zebrafish experiments were performed in strict accordance of guidelines from the University of Utah Institutional Animal Care and Use Committee (IACUC), regulated under federal law (the Animal Welfare Act and Public Health Services Regulation Act)

by the U.S. Department of Agriculture (USDA) and the Office of Laboratory Animal Welfare at the NIH, and accredited by the Association for Assessment and Accreditation of Laboratory Care International (AAALAC).

Fish stocks and embryo raising

Adult fish were bred according to standard methods. Embryos were raised at 28.5°C in E3 embryo medium and staged by time and morphology. For *in situ* staining and immunohistochemistry, embryos were fixed in 4% paraformaldehyde (PFA) in 1x PBS overnight at 4°C, washed briefly in 1xPBS with 0.1% Tween-20, serially dehydrated, and stored in 100% MeOH at -20°C until use. Transgenic fish line and alleles used in this paper were the following: Tg(*olig2:dsRed)*^{vu19}.[20]

***Lsm7* sequence analysis and construct generation**

Human and zebrafish Lsm7 amino acid sequences were aligned using PRALINE. The construct for the *lsm7* riboprobe was amplified by PCR using Phusion® High-Fidelity DNA Polymerases (New England Biolabs, NEB) with primers: *lsm7* forward (5'-GGATCCGCCGCCACCATGGCGGACAAAGACAAGAAAAAGAAGGAG-3') and *lsm7* reverse (5'- CTCAAGGCGTCCAGTAACCAAAGCCC-3').

The constructs of human LSM7$^{full\text{-}length}$, LSM7^{D41N}, and LSM7^{R69P} for capped RNA synthesis were amplified from p3XFlag-CMV-LSM7$^{full\text{-}length}$, p3XFlag-CMV-LSM7^{D41N}, and p3XFlag-CMV-LSM7^{R69P}, respectively, by PCR using Phusion® High-Fidelity DNA Polymerases with the following primers: *LSM7* forward (5'-GAATTCGCCGCCACCATGGCGGATAAGGAGAAGAAGAAAAAG-3') and *LSM7*

reverse (5’- GAATTCCTACTTGTCATCGTCATCCTTGTAGTC -3’), and then subcloned into pCS2^{+} vector.

lsm7 CRISPR sgRNA construction and injection

We designed sgRNA target sites for the zebrafish *lsm7* gene (Ensembl Zv11: ENSDART00000081188.7) by looking for sequences corresponding to GGN$_{18}$nGG on the sense or antisense strand using the CRISPR design program CHOPCHOP.[21] Off-target effects were checked with NIH BLAST tool applied to the zebrafish genome (zv11). Off-target sequences that had significant matches of the final 23 nt of the target and NGG PAM sequence were discarded. DNA template for *lsm7* exon3 sgRNA was amplified by PCR using Phusion® High-Fidelity DNA Polymerases with *lsm7* exon3 specific forward primer (5’-GAAATTAATACGACTCACTATACCCGTTGTTGAATCTTGTGTGTTTTAGAGCTAGAAATAGC -3’) and universal reverse primer (5’-AAAAGCACCGACTCGGTGCCACTTTTTCAAGTTGATAACGGACTAGCCTTATTTTAACTTGCTATTTCTAGCTCTAAAAC -3’). The PCR program used for template synthesis was 98°C 30 seconds, 35 cycles of [98°C 10 seconds, 60°C 30 seconds, 72°C 15 seconds], 72°C 10 minutes, 10°C end. Subsequently, the DNA template was purified by QIAquick PCR Purification Kit (Qiagen). The *lsm7 exon3* sgRNA was synthesized by the HiScribe T7 RNA Synthesis kit (BioLabs) followed by RNA purification with RNA Clean & Concentrator-5 (Zymo research).

The *lsm7* exon3 sgRNA (460 pg) and Cas9 protein (460 pg, PNA BIO) were injected into one cell stage embryos. CRISPR efficiency was evaluated on individual 24 hpf

injected embryos after DNA extraction, PCR amplification of the target locus, and HRMA analysis. A *lsm7* exon3 sgRNA dose of 460 pg resulted in >90% mutagenesis in 24 hpf embryos, assayed by high-resolution melt analysis.[22] Embryos used for injection were derived from either wild-type AB parents or Tg(*olig2:dsRed)*^{vu19} as mentioned in the text.

Capped RNA synthesis

Capped RNA encoding the full coding sequence of LSM7$^{full\text{-}length}$, LSM7^{Asp41Asn}, or LSM7^{Arg69Pro} were prepared as per manufacturer's instructions and purified with Micro Bio-spin 6 columns (BioRad). Capped RNAs (460 pg) were injected for rescue experiments.

Immunohistochemistry and in situ hybridization

Immunohistochemistry was performed as previously described.[23] Antibodies used were rabbit anti-dsRed 1:250 (Clontech), Alexa 555 goat anti-rabbit 1:400 (ThermoFisher Scientific), and 4',6-diamidino-2-phenylindole (DAPI). The antisense digoxigenin-UTP labeled riboprobe for detecting *lsm7* transcript was synthesized according to manufacturer's instructions (Roche), and *in situ* hybridizations were performed as described previously.[24] The color reaction was carried out using NBT/BCIP substrate (Roche).

Morphological analysis

5 dpf fish larvae were fixed in 4% PFA in 1x PBS overnight at 4°C, washed briefly in 1xPBS with 0.1% Tween-20. One eye of an individual larva was dissected out and mounted laterally. Eyes were imaged, and the length was measured from anterior to posterior along the longest axis by ImageJ software.

Behaviour analysis

Larval behaviour analysis was performed on 7 dpf larvae in 96-well square bottom plates (Krackeler Scientific) using video analysis software (Noldus EthoVision). For spontaneous behaviour, animals were transferred at 6 dpf to a 96-well plate and kept at 28.5˚C overnight. At 7 dpf the plate was placed on the video imaging system and animals were allowed to adapt in the dark for 10 minutes, and then recording was performed for 5 minutes (1 minute dark and 4 minutes light).

Microscopy and image analysis

Immunostained embryos were transferred step-wise into 90% glycerol/10% PBS, mounted on a glass slide with a #0 coverslip, and imaged on a confocal microscope. Confocal stacks were projected in ImageJ, and images composed with Adobe Photoshop and Illustrator.

TUNEL quantification

Terminal deoxynucleotidyl transferase dUTP nick-end labeling (TUNEL) was performed on whole-mount larvae (ApopTag Fluorescein *In Situ* Apoptosis Detection Kit; Millipore)

as previously described.[25] Confocal imaging was performed, and images were rendered in ImageJ by compiling an average intensity projection of 120 µm (step size 5 µm) into a single z-stack image, for cell counting using Photoshop's (Adobe) count tool.

Statistical analysis

qPCR data were analyzed following the MIQE guidelines and expressed as average relative normalized expression with appropriate error bars (SEM). Normality of all data were assessed using the Shapiro-Wilks Test of Normality and the equality of variances were assessed using Levene's Test. Changes in *LSM7* mRNA levels in individual 1 compared to controls were analyzed using a parametric, unpaired *t*-test (two-tailed). Changes in LSM7 protein levels in individual 1 compared to controls were analyzed using a parametric, unpaired *t*-test (two tailed). Statistical significance was set at $p < 0.05$. Statistical analyses for zebrafish experiments were performed using Prism8 software (GraphPad). Student's *t*-test was used for two-way comparisons; comparisons between three or more groups was performed with ANOVA with post-hoc Tukey's HSD between individual means.

Supplemental References:

1. Retterer, K., Juusola, J., Cho, M.T., Vitazka, P., Millan, F., Gibellini, F., Vertino-Bell, A., Smaoui, N., Neidich, J., Monaghan, K.G., et al. (2016). Clinical application of whole-exome sequencing across clinical indications. Genet Med 18, 696-704.
2. Richards, S., Aziz, N., Bale, S., Bick, D., Das, S., Gastier-Foster, J., Grody, W.W., Hegde, M., Lyon, E., Spector, E., et al. (2015). Standards and guidelines for the interpretation of sequence variants: a joint consensus recommendation of the American College of Medical Genetics and Genomics and the Association for Molecular Pathology. Genet Med 17, 405-424.
3. Monies, D., Abouelhoda, M., Assoum, M., Moghrabi, N., Rafiullah, R., Almontashiri, N., Alowain, M., Alzaidan, H., Alsayed, M., Subhani, S., et al. (2019). Lessons Learned from Large-Scale, First-Tier Clinical Exome Sequencing in a Highly Consanguineous Population. Am J Hum Genet 105, 879.
4. Taylor, S., Wakem, M., Dijkman, G., Alsarraj, M., and Nguyen, M. (2010). A practical approach to RT-qPCR-Publishing data that conform to the MIQE guidelines. Methods 50, S1-5.
5. Taylor, S.C., and Mrkusich, E.M. (2014). The state of RT-quantitative PCR: firsthand observations of implementation of minimum information for the publication of quantitative real-time PCR experiments (MIQE). J Mol Microbiol Biotechnol 24, 46-52.
6. Zhou, L., Hang, J., Zhou, Y., Wan, R., Lu, G., Yin, P., Yan, C., and Shi, Y. (2014). Crystal structures of the Lsm complex bound to the 3' end sequence of U6 small nuclear RNA. Nature 506, 116-120.
7. Chen, G.I., and Gingras, A.C. (2007). Affinity-purification mass spectrometry (AP-MS) of serine/threonine phosphatases. Methods 42, 298-305.
8. Mellacheruvu, D., Wright, Z., Couzens, A.L., Lambert, J.P., St-Denis, N.A., Li, T., Miteva, Y.V., Hauri, S., Sardiu, M.E., Low, T.Y., et al. (2013). The CRAPome: a contaminant repository for affinity purification-mass spectrometry data. Nature methods 10, 730-736.
9. Cox, J., and Mann, M. (2008). MaxQuant enables high peptide identification rates, individualized p.p.b.-range mass accuracies and proteome-wide protein quantification. Nat Biotechnol 26, 1367-1372.
10. Cox, J., Michalski, A., and Mann, M. (2011). Software lock mass by two-dimensional minimization of peptide mass errors. J Am Soc Mass Spectrom 22, 1373-1380.
11. Cox, J., Hein, M.Y., Luber, C.A., Paron, I., Nagaraj, N., and Mann, M. (2014). Accurate proteome-wide label-free quantification by delayed normalization and maximal peptide ratio extraction, termed MaxLFQ. Mol Cell Proteomics 13, 2513-2526.
12. Schaab, C., Geiger, T., Stoehr, G., Cox, J., and Mann, M. (2012). Analysis of high accuracy, quantitative proteomics data in the MaxQB database. Mol Cell Proteomics 11, M111 014068.
13. Tyanova, S., Temu, T., Carlson, A., Sinitcyn, P., Mann, M., and Cox, J. (2015). Visualization of LC-MS/MS proteomics data in MaxQuant. Proteomics 15, 1453-1456.

14. Tyanova, S., Temu, T., and Cox, J. (2016). The MaxQuant computational platform for mass spectrometry-based shotgun proteomics. Nat Protoc 11, 2301-2319.
15. Tyanova, S., Temu, T., Sinitcyn, P., Carlson, A., Hein, M.Y., Geiger, T., Mann, M., and Cox, J. (2016). The Perseus computational platform for comprehensive analysis of (prote)omics data. Nat Methods 13, 731-740.
16. Rudolph, J.D., and Cox, J. (2019). A Network Module for the Perseus Software for Computational Proteomics Facilitates Proteome Interaction Graph Analysis. J Proteome Res 18, 2052-2064.
17. Tyanova, S., Albrechtsen, R., Kronqvist, P., Cox, J., Mann, M., and Geiger, T. (2016). Proteomic maps of breast cancer subtypes. Nat Commun 7, 10259.
18. Cox, J., and Mann, M. (2012). 1D and 2D annotation enrichment: a statistical method integrating quantitative proteomics with complementary high-throughput data. BMC Bioinformatics 13 Suppl 16, S12.
19. Choquet, K., Pinard, M., Yang, S., Moir, R.D., Poitras, C., Dicaire, M.J., Sgarioto, N., Lariviere, R., Kleinman, C.L., Willis, I.M., et al. (2019). The leukodystrophy mutation Polr3b R103H causes homozygote mouse embryonic lethality and impairs RNA polymerase III biogenesis. Mol Brain 12, 59.
20. Kucenas, S., Takada, N., Park, H.C., Woodruff, E., Broadie, K., and Appel, B. (2008). CNS-derived glia ensheath peripheral nerves and mediate motor root development. Nat Neurosci 11, 143-151.
21. Labun, K., Montague, T.G., Krause, M., Torres Cleuren, Y.N., Tjeldnes, H., and Valen, E. (2019). CHOPCHOP v3: expanding the CRISPR web toolbox beyond genome editing. Nucleic Acids Res 47, W171-W174.
22. Xing, L., Quist, T.S., Stevenson, T.J., Dahlem, T.J., and Bonkowsky, J.L. (2014). Rapid and efficient zebrafish genotyping using PCR with high-resolution melt analysis. J Vis Exp, e51138.
23. Bonkowsky, J.L., Wang, X., Fujimoto, E., Lee, J.E., Chien, C.B., and Dorsky, R.I. (2008). Domain-specific regulation of foxP2 CNS expression by lef1. BMC Dev Biol 8, 103.
24. Thisse, C., and Thisse, B. (2008). High-resolution in situ hybridization to whole-mount zebrafish embryos. Nat Protoc 3, 59-69.
25. Lambert, A.M., Bonkowsky, J.L., and Masino, M.A. (2012). The conserved dopaminergic diencephalospinal tract mediates vertebrate locomotor development in zebrafish larvae. J Neurosci 32, 13488-13500.